Received: 9 October 2023 | Revised: 15 February 2024 | Accepted: 17 February 2024

DOI: 10.1111/jnc.16089

Journal of Neurochemistry JNC The Official Journal of the International Society for Neurochemistry WILEY

ORIGINAL ARTICLE

# Regulation of astrocyte metabolism by mitochondrial translocator protein 18 kDa

Wyn Firth | Josephine L. Robb | Daisy Stewart | Katherine R. Pye | Rosemary Bamford | Asami Oguro-Ando | Craig Beall | Kate L. J. Ellacott

Department of Clinical and Biomedical Sciences, University of Exeter Medical School, Faculty of Health and Life Sciences, University of Exeter, Exeter, UK

**Correspondence**
Kate L. J. Ellacott, Department of Clinical and Biomedical Sciences, University of Exeter Medical School, Faculty of Health and Life Sciences, University of Exeter, Exeter, UK.
Email: k.ellacott@exeter.ac.uk

**Present address**
Josephine L. Robb, Université de Montréal, Montreal, Quebec, Canada.

**Funding information**
Medical Research Council, Grant/Award Number: MR/R014345/1; Research England; British Society for Neuroendocrinology

## Abstract

The mitochondrial translocator protein 18 kDa (TSPO) has been linked to functions from steroidogenesis to regulation of cellular metabolism and is an attractive therapeutic target for chronic CNS inflammation. Studies in Leydig cells and microglia indicate that TSPO function may vary between cells depending on their specialized roles. Astrocytes are critical for providing trophic and metabolic support in the brain. Recent work has highlighted that TSPO expression increases in astrocytes under inflamed conditions and may drive astrocyte reactivity. Relatively little is known about the role TSPO plays in regulating astrocyte metabolism and whether this protein is involved in immunometabolic processes in these cells. Using TSPO-deficient ($TSPO^{-/-}$) mouse primary astrocytes in vitro (MPAs) and a human astrocytoma cell line (U373 cells), we performed extracellular metabolic flux analyses. We found that TSPO deficiency reduced basal cellular respiration and attenuated the bioenergetic response to glucopenia. Fatty acid oxidation was increased, and lactate production was reduced in $TSPO^{-/-}$ MPAs and U373 cells. Co-immunoprecipitation studies revealed that TSPO forms a complex with carnitine palmitoyltransferase 1a in U373 and MPAs, presenting a mechanism wherein TSPO may regulate FAO in these cells. Compared to $TSPO^{+/+}$ cells, in $TSPO^{-/-}$ MPAs we observed attenuated tumor necrosis factor release following 3 h lipopolysaccharide (LPS) stimulation, which was enhanced at 24 h post-LPS stimulation. Together these data suggest that while TSPO acts as a regulator of metabolic flexibility, TSPO deficiency does not

**Abbreviations:** −/−, Knockout; deficient; +/+, Wildtype; expressing; 2DG, 2-deoxyglucose; ADAM17, A disintegrin and metalloprotease 17; ANOVA, Analysis of variance; ASPA, Animals (Scientific Procedures) Act 1986; ATP, Adenosine triphosphate; B, Bound fraction; BSA, Bovine serum albumin; C16, Palmitate; CNS, Central nervous system; Co-IP, Co-immunoprecipitation; CPT1a, Carnitine palmitoyltransferase 1a; CRISPR-Cas9, Clustered regularly interspaced palindromic repeats-CRISPR associated protein 9; Ctrl, Vehicle-treated control; DBM-PBS, n-dodecyl-β-maltoside phosphate buffered saline; ddH2O, Double distilled water; DMEM, Dulbecco's modified Eagle's medium; DMSO, Dimethyl sulfoxide; ECACC, European Collection of Authenticated Cell Cultures; ECAR, Extracellular acidification rate; EFA, Extracellular flux analysis; ELISA, Enzyme-linked immunosorbent assay; Elu, Eluate; Eto, Etomoxir; EV, Empty vector; FAO, Fatty acid oxidation; FBS, Fetal Bovine Serum; FCCP, Carbonyl cyanide-4 (trifluoromethoxy) phenylhydrazone; GAPDH, Glyceraldehyde 3-phosphate dehydrogenase; GFAP, Glial fibrillary acidic protein; Gluc, Glucose; GLUT1, Glucose transporter 1; HEPES, 4-(2-hydroxyethyl)-1-piperazineethanesulfonic acid; HK2, Hexokinase 2; I, Input; IB, Immunoblot; IgG, Immunoglobulin G; IPs, Immunoprecipitations; kDa, Kilodaltons; L, Ladder; LED, Light emitting diode; LPS, Lipopolysaccharide; Lys, Lysate; mM, Millimolar; MPA(s), Mouse primary astrocyte(s); Myc, Myelocytomatosis oncogene; NDS, Normal donkey serum; NFκB, Nuclear factor kappa B; NLRP3, Nod-like receptor family pyrin domain containing 3; OCR, Oxygen consumption rate; Oligo, Oligomycin; PBS, Phosphate buffered saline; pCMV, Porcine cytomegalovirus; PCR, Polymerase chain reaction; PLL, Poly-L-lysine; R/A, Rotenone/antimycin A; RIPA, Radioimmunoprecipitation; RRID, Research resource identifier (see scicrunch.org); RTP, Room temperature and pressure; SDS, Sodium dodecyl sulfate; SEM, Standard error of the mean; STR-PCR, Short tandem repeat polymerase chain reaction; TBS, Tris-buffered saline; TBS-T, TBS-Tween 20; TNF, Tumor necrosis factor; TSPO, Translocator protein 18 kDa; UB, Unbound fraction; VDAC, Voltage-dependent anion channel.

appear to modulate the metabolic response of MPAs to inflammation, at least in response to the model used in this study.

**KEYWORDS**
astrocyte, cytokine release, fatty acid oxidation, inflammation, metabolism, TSPO

## 1 | INTRODUCTION

The mitochondrial translocator protein 18 kDa (TSPO) is a pentameric transmembrane protein with a high degree of evolutionary conservation (Bonsack & Sukumari-Ramesh, 2018; Hiser et al., 2021; Lee et al., 2020) that resides on the outer mitochondrial membrane of mammalian cells (Fan et al., 2012; Selvaraj & Tu, 2016), including glia (Kuhlmann & Guilarte, 2000). TSPO has been linked to various functions including cholesterol transport into the mitochondria (Bonsack & Sukumari-Ramesh, 2018; Fan et al., 2012; Selvaraj & Tu, 2016), steroidogenesis (Bonsack & Sukumari-Ramesh, 2018; Fan et al., 2012; Lee et al., 2020; Selvaraj & Tu, 2016), inflammatory responses (Downer et al., 2020; Kim et al., 2020; Selvaraj & Tu, 2016), phagocytosis (Fairley et al., 2023; Yao et al., 2020; Zhang et al., 2021), reactive oxygen species production (Guilarte et al., 2016; Wolf et al., 2020), and regulation of cellular metabolism (Betlazar et al., 2020; Selvaraj & Tu, 2016; Tu et al., 2014). This array of functions is highly relevant to glial cells, and while there is some knowledge about the role of TSPO in microglia, less is known about its role in astrocytes.

The brain is a metabolically expensive system with the highest weight-to-energy-use ratio of any organ in the body (Raichle & Gusnard, 2002). It is therefore essential that energy use in the CNS is tightly controlled. Astrocytes play key roles in nutrient uptake and distribution (Abbott et al., 2006; Cabezas et al., 2014; Verkhratsky & Nedergaard, 2018), forming intimate relationships with neurons to provide trophic support and modulate neuronal activity directly; in turn, experimental modulation of these cells is sufficient to alter behavioral outputs (González-García et al., 2021; Park & Lee, 2020; Verkhratsky & Nedergaard, 2018). In concert with microglia, astrocytes participate in the CNS inflammatory response by detecting and repairing damage, though this is not considered to be their primary function (Escartin et al., 2021; Liddelow et al., 2017, 2020). As inflammation requires changes in cellular metabolism, this affects energy use within the CNS (Killen et al., 2019; Robb et al., 2019; Yin et al., 2016). We have previously shown that acute and chronic inflammation differentially alters the metabolic phenotype of primary mouse astrocytes in culture, modulating their expression of proteins involved with nutrient sensing and uptake, such as glucose transporter 1 (GLUT1) (Robb et al., 2020).

Previous work has demonstrated that chronic inflammation in the CNS is linked to upregulated TSPO expression (Guilarte et al., 2022), which has been largely attributed to glial cells (Fairley et al., 2021, 2023; Fu et al., 2020; Yao et al., 2020). In addition to regulating inflammatory responses, TSPO has been implicated in the regulation of cellular metabolism in the CNS and the periphery. For example, in 2016, Tu et al. (2016). provided evidence that TSPO may act as a regulator of fatty acid oxidation (FAO) in MA-10 Leydig cells, demonstrating that in these cells TSPO deficiency upregulates gene expression of carnitine palmitoyltransferase 1a (*Cpt1a*), which encodes the rate-limiting enzyme of FAO. This study also showed that overexpression of TSPO downregulates *Cpt1a* expression, suggesting a bidirectional relationship (Tu et al., 2016). Using murine microglia, a related study showed that in addition to metabolic impairments, microglial activation in response to proinflammatory stimulation is impaired by TSPO deficiency (Yao et al., 2020). More recently, Fairley et al. (2023) demonstrated that TSPO regulates glycolytic enzyme function and phagocytosis in microglia. However, in GBM1B stem-like cells and U87MG glioma cells, TSPO knockdown has been shown to increase glycolysis and reduce mitochondrial respiration (Fu et al., 2020). The heterogeneity in these findings implies that TSPO may play cell-type and state-dependent roles in regulating cellular metabolism.

Studies on the role of TSPO in astrocytes are necessary because of the developmental and functional distinctions between astrocytes and microglia (Bernier et al., 2020; Kriegstein & Alvarez-Buylla, 2009; Wurm et al., 2021) including differential expression of metabolic enzymes, such as CPT1a which is expressed to a much greater extent in astrocytes (Bernier et al., 2020; Jernberg et al., 2017). Their unique functions require astrocytes to have fine control of energy sensing and cellular metabolism to rapidly respond to stimuli and restore the homeostatic balance of the brain. TSPO has received attention as a potential therapeutic target for neuroinflammatory conditions given its potential role at the interface of inflammatory responses and metabolism ('immunometabolism') in glia (Dimitrova-Shumkovska et al., 2020; Fairley et al., 2023; Li et al., 2017). While it was recently shown that the astrocyte response to inflammatory stimuli includes regulation of TSPO expression (Tournier et al., 2023), the role TSPO plays in regulating astrocyte basal metabolism, inflammatory responses, and the metabolic response of astrocytes to inflammatory stimulation remains unclear.

Our work tested the hypothesis that TSPO deficiency impairs astrocyte glucose metabolism and enhances FAO-based metabolism under basal conditions. We investigated a possible mechanistic basis for this using co-immunoprecipitations, elucidating a mechanism by which TSPO may regulate astrocyte metabolism. The impact of TSPO deficiency on the metabolic responses of astrocytes to an inflammatory stimulus was also explored.

## 2 | METHODS

Unless otherwise stated, reagents were obtained from Fisher Scientific (UK).

### 2.1 | Animal use and husbandry

All animal studies were conducted in accordance with the UK Animals (Scientific Procedures) Act 1986 (ASPA; project license PP5594553) and study plans were approved by the institutional Animal Welfare and Ethical Review Body at the University of Exeter. Mice were group housed on a 12:12 light–dark cycle at 22 ± 2°C with ad libitum access to standard laboratory rodent diet (LabDiet [EU] Rodent diet 5LF2; LabDiet, London, UK) and water.

As detailed in Morrissey et al. (2021), mating pairs of TSPO heterozygote ($^{+/-}$) (Tspo$^{tm1b(EUCOMM)Wtsi}$) mice were used to produce the homozygote knockout (TSPO$^{-/-}$) and wildtype (TSPO$^{+/+}$) littermate neonates from which TSPO$^{+/+}$ and TSPO$^{-/-}$ primary astrocytes were isolated for use in these studies. Mice were crossed >7 generations onto a C57BL/6J background.

Mating pairs of C57BL/6J mice (Research Resource Identifier [RRID]: IMSR_JAX:000664; Charles River, UK) were bred to produce mouse pups from which primary astrocytes were isolated. Data from this strain are presented in Figures 7 and 8.

Offspring of both sexes were used in these studies. All cells generated from mouse neonates were evenly distributed into control and experimental groups. A total of 282 neonates were used to generate the cells used in this study. No experimental animals were excluded from the study.

### 2.2 | Genotyping

TSPO genotypes ($^{+/+}$, $^{+/-}$, $^{-/-}$) of breeder mice and mouse primary astrocytes (MPAs) were determined by PCR as reported previously in Morrissey et al. (2021) (Figure S1).

### 2.3 | Isolation of primary astrocytes and general cell culture

All cell cultures were maintained in 25 mM glucose Dulbecco's modified Eagle's medium (DMEM; catalog number D5671, Merck Millipore [UK]) with 10% (v/v) Fetal Bovine Serum (FBS; catalog number 10270106), 8 mM L-glutamine (catalog number 11500626) and 2% (v/v) penicillin–streptomycin (catalog number 11528876). Cultures were maintained in humidified incubators at 37°C with 5% $CO_2$.

U373 astrocytoma cells were purchased from the European Collection of Authenticated Cell Cultures (U-373 MG [Uppsala] [ECACC 08061901]; RRID:CVCL_2818). The identity of the U373 cells was verified and authenticated by STR-PCR profiling, which was performed by the ECACC. The U373 cells used in this study were the original cell line established in 1973. U373 astrocytoma cells that were not subject to previous genetic modification were maintained up to a maximum of passage (p) 30 for use in these studies. TSPO$^{-/-}$ and empty vector wildtype control U373 astrocytoma cells were used up to a maximum of p65. Though not ideal, this high passage number was unavoidable due to expanding single-cell colonies following genetic modification with the CRISPR-Cas9 system.

Mouse primary astrocytes (MPAs) were isolated from cortical tissue of neonates (postnatal days 1–5) following euthanasia via rapid decapitation without anesthesia as previously published (Robb et al., 2020). All plastic and glassware used to culture MPAs was coated with poly-L-lysine (PLL; 4 μg/mL; catalog number P1274, Merck Millipore [UK]). TSPO$^{-/-}$ MPAs were grown in T25 flasks (one brain per flask) until confluent before being stored in liquid nitrogen in single vials (10% v/v dimethyl sulfoxide [DMSO; catalog number D2650, Merck Millipore (UK)]) until TSPO genotypes had been confirmed. Once thawed, up to five vials of MPAs of the same TSPO genotype were pooled together into a T75 flask and grown until 100% confluent. MPAs from wildtype C57BL/6J neonates were grown in T75 flasks (2–3 brains per flask) until confluent. Once confluent, MPAs were stored in liquid nitrogen (10% DMSO). Immunocytochemistry was used to assess astrocyte purity via presence of glial fibrillary acidic protein (GFAP) immunoreactivity. Manual counting determined that astrocyte purity was ≥92% with a mean purity of 98.67 ± 1.61% across all coverslips counted (Figure S2; $n = 10$ coverslips, 2–5 images per coverslip over 3–4 individual collections).

The day before experiments, MPAs or U373 cells were seeded in DMEM (catalog number 11966) with 7.5 mM glucose (catalog number G7021, Merck Millipore [UK]), 10% (v/v) FBS, 8 mM L-glutamine and 2% (v/v) penicillin–streptomycin. On the day of experiments involving treatments, cells were cultured in serum-free DMEM (catalog number 11966) supplemented with 2.5 mM glucose for 2 h before treatments were applied in the same media. When performing extracellular metabolic flux analyses or measuring metabolite production, XF DMEM (pH 7.4) (catalog number 103575–100; Agilent, UK) with 2.5 mM glucose, 2.5 mM sodium pyruvate, and 2 mM L-glutamine was used. As cells of the same TSPO genotype isolated from different neonates were pooled together, *n* was treated as one well/dish for the purposes of this study. A minimum of three biological replicates were collected per experiment. For extracellular flux analysis experiments, *n* was treated as one well per 96-well plate because each well was regarded as a distinct microenvironment. These experiments were repeated over 2–3 distinct 96-well plates on separate days with cells derived from distinct culture flasks isolated from separate animals.

### 2.4 | Generation of TSPO-deficient U373 cells

Guide RNAs for TSPO were designed against Exons 2 and 3 of *Tspo* (Ensembl transcript: ENST00000396265.4 TSPO-203) using Benchling (Benchling software, 2019; RRID:SCR_013955) and cloned into either a pSpCas9(BB)-2A-GFP (PX458; Addgene

plasmid #48138; RRID:Addgene_159654) plasmid or a pU6-(BbsI)_CBh-Cas9-T2A-mCherry plasmid (Addgene plasmid #64324; RRID:Addgene_64324) according to the method published by Ran et al (2013). Plasmids validated by Sanger sequencing (Genewiz, Azenta Life Sciences Ltd, UK) were co-transfected into U373 cells using Lipofectamine LTX alongside a non-coding guide ('empty vector', EV) control prior to clonal selection. TSPO genotype was confirmed by PCR and Western blotting (Figure S3). See Supplementary Methods for full gRNA details (Table S1) and primer sequences (Table S2).

## 2.5 | Bacterial transformations and U373 transfections

Plasmids (Myc-tagged TSPO ['TSPO-Myc'; catalog number RC220107, OriGene] or a pCMV backbone non-coding EV control [catalog number PS100001, OriGene]) were grown in chemically competent DH5α *E. coli* following transformation via heat shock. Then, 25 μg/mL kanamycin (catalog number K4000, Merck Millipore [UK]) was used to select successful transformants. Plasmids were extracted using a Plasmid Midi Kit (catalog number 12143, Qiagen) according to the manufacturer's specifications with the following modification: all centrifugation steps took place at 4600×*g* at room temperature and pressure (RTP) with appropriate modifications to the duration of spins (step 1: 15 min; step 10: 35 min; step 11: 15 min). Plasmids were allowed to air dry in a fume hood for 15 min before resuspension in 500 μL Buffer TE (Qiagen). Plasmid concentration was quantified using a Nanodrop 2000.

U373 cells were transiently transfected in 6-well plates with 2.5 μg plasmid (TSPO-Myc or pCMV EV) per well using Lipofectamine 3000 (catalog number 15292465) according to the manufacturer's specifications with minor modifications: transfection complexes were made up using serum-free D5671 DMEM with 8 mM L-glutamine and 2% (v/v) penicillin–streptomycin 10 min before use. Cells in DMEM (catalog number 11966) with 7.5 mM glucose, 10% (v/v) FBS, 8 mM L-glutamine and 2% (v/v) penicillin–streptomycin were seeded directly into transfection complex mixes and left for 24 h before cell lysates were harvested.

## 2.6 | Cell treatments

Prior to treatment, cells were washed once with 0.01 M phosphate-buffered saline (PBS; catalog number 10209252) and incubated in serum-free 2.5 mM glucose DMEM (catalog number 11966) ('assay media') for 2 h. Treatments were diluted to the appropriate concentrations in assay media immediately before application. 2-deoxyglucose (2DG; catalog number D8375-5G, Merck Millipore UK; reconstituted in $ddH_2O$) was diluted to a working concentration of 10 mM. Lipopolysaccharide from *Escherichia coli* (LPS; 026:B6; catalog number L8274, Merck Millipore [UK]; reconstituted in $ddH_2O$) was diluted to a working concentration of 100 ng/mL.

## 2.7 | Protein quantification

Cell lysates for immunoblotting studies were collected using modified RIPA buffer (Table S3) and manual scraping. Collected lysates were frozen, thawed on ice and centrifuged at 21000×*g* for 20 min at 4°C. Protein content of supernatant was quantified via Bradford assay according to the manufacturer's instructions (catalog number 500-0006, Bio-Rad). Absorbance was measured at 595 nm using a Pherastar FS (BMG LABTECH).

## 2.8 | Co-immunoprecipitation

### 2.8.1 | Immunoprecipitation of lysate from transfected cells

Co-immunoprecipitations were performed using Myc-Trap agarose beads (catalog number yta-20, Proteintech) according to the manufacturer's specifications with minor modifications: 20 μL beads were used per tube; following the final wash/spin step, complexes were eluted in 2X SDS sample buffer (62.5 mM Tris–HCl [pH 6.8], 2% SDS, 10% glycerol, bromophenol blue) by boiling at 95°C for 10 min. The eluate was centrifuged at 2500×*g* for 5 min at 4°C and samples were stored at −70°C until use in immunoblotting.

### 2.8.2 | Immunoprecipitation of endogenous proteins from non-transfected cells

Cells (U373 cells or MPAs) were seeded at $3.0 \times 10^6$ cells per dish in 150 mm dishes. The next day, cells were lysed with ice-cold immunoprecipitation buffer (Table S4). Cell lysates were homogenized by turning 30 times in a Dounce homogenizer. Lysate was centrifuged at 1000×*g* for 10 min (4°C) before quantification via Bradford assay. For immunoprecipitations (IPs) using U373 cell lysate, 400 μg protein was loaded per IP. For IPs using MPA lysate, 200–400 μg protein was loaded per IP. Protein G Dynabeads (catalog number 10003D) were washed with 0.02% (v/v) PBS-Tween 20 (Tween-20: catalog number P2285, Merck Millipore; 0.01 M PBS) and incubated with 200 μL of primary antibody mix (for antibody details see Table S5) for 1 h (RTP) on a rotary mixer. The supernatant was discarded and beads washed three times in 0.02% PBS-Tween prior to incubation with cell lysate diluted in 0.01% (v/v) n-dodecyl-β-maltoside (catalog number 89902) in PBS (DBM-PBS; 0.01 M PBS) on a rotary mixer for 2 h (4°C). Supernatant was moved to a clean tube and 50 μL 4X SDS sample buffer (125 mM Tris–HCl [pH 6.8], 4% SDS, 20% glycerol, bromophenol blue) was added. This 'unbound fraction' was incubated at 70°C for 5 minutes. Meanwhile, beads were washed three times with DBM-PBS, moved to a fresh tube, and the bound protein was eluted using 50 μL 4X SDS sample buffer and heating at 70°C for 5 min. Immunoblotting was used to identify proteins of interest.

## 2.9 | Immunoblotting

Following sample collection and co-immunoprecipitation (co-IP) (where applicable), samples were loaded onto 15% (v/v) polyacrylamide gels. In co-IP studies using samples from transfected cells, 20 μL per fraction was loaded per well. In co-IP studies using endogenous protein, 12.5 μL per fraction was loaded per well. To generate semi-quantifiable immunoblots, 10 μg protein was loaded per well where relevant (i.e., in all immunoblots except for co-IP studies). Samples were run at 90 V for 15 min to clear stacking gels, immediately followed by running at 150 V for 90 min through the resolving gels. At the end of the run, polyacrylamide gels were transferred onto nitrocellulose membranes (catalog number 732-3031, VWR) via wet transfer at 100 V for 70 min. Membranes were blocked using Odyssey blocking buffer (Tris-buffered saline [TBS]) (catalog number 927-50000; Licor, UK) for 1 h (RTP). Primary antibodies were applied overnight at 4°C or for 1 h at RTP. Membranes were washed three times in TBS (20 mM Tris–HCl [pH 7.4], 152 mM NaCl) with 0.05% (v/v) Tween-20 (TBS-T) before application of secondary antibodies. See Supplementary Methods (Table S6) for antibody details. Membranes were scanned using an Odyssey CLx scanner (Licor, UK). Bands for proteins of interest were normalized to the expression of GAPDH and data expressed as fold change over control.

## 2.10 | Immunocytochemistry

Cells were seeded onto PLL-coated coverslips at a density of $1\times10^5$ cells per coverslip and left overnight. Cells were washed with 0.01 M PBS and incubated (37°C, 5% $CO_2$) in assay media for 2 h prior to fixation by immersion in ice-cold methanol (catalog number 34860-2.5L-R, Merck Millipore [UK]) for ~90 s. Methanol was removed and coverslips were washed thrice with 0.01 M PBS before blocking in 5% (v/v) normal donkey serum (NDS; catalog number S30-100 mL, Merck Millipore [UK]) in 0.01 M PBS (3% Tween-20) for 15 min at RTP. Coverslips were then incubated with primary antibodies for 15 min (RTP) before being stored at 4°C overnight (18–20 h). The next day, primary antibodies were removed and coverslips washed three times with PBS. Secondary antibodies were applied for 1 h RTP in darkness. See Supplementary Methods (Table S7) for antibody details. Coverslips were allowed to air dry in darkness before being mounted onto slides using Fluoroshield Mounting Medium with DAPI (catalog number AB104139-20ML, Abcam, UK). Slides were imaged using a DM4000 B LED Fluorescent microscope.

## 2.11 | Extracellular metabolic flux analyses

Cells were seeded at a density of $4\times10^4$ cells per well in 96 well plates 20–24 h prior to experimentation. XF DMEM was used for all metabolic flux assays. Media were supplemented as appropriate for the assay used: for basal measurements of cellular metabolism in the presence of glucose and the mitochondrial stress test, XF DMEM was supplemented with 2.5 mM glucose (catalog number G7021, Merck Millipore [UK]), 2.5 mM sodium pyruvate (catalog number P2256, Merck Millipore [UK]), and 2 mM L-glutamine (catalog number 11500626); for the glycolysis stress test, XF DMEM was supplemented with 2 mM L-glutamine; for measurements of cellular metabolism in the absence of glucose XF DMEM was supplemented with 2.5 mM sodium pyruvate and 2 mM L-glutamine. Prior to assays, cells were washed once with XF DMEM (containing supplements relevant to the test used). Cells were placed into a humidified non-$CO_2$ incubator at 37°C to 'degas' for 60 min immediately prior to the assays. Following the degas period, cells were placed into the XFe96 bioanalyzer (Agilent) and assays commenced. Readings were taken over 3-min mix-measure cycles during the assay, with 3–4 measurements per cycle. A baseline read of 3–4 cycles was taken prior to any injections.

### 2.11.1 | Mitochondrial stress test

The mitochondrial stress test was performed according to the manufacturer's instructions (catalog number 103015-100, Agilent, UK) with minor modifications. Following the initial baseline reads, oligomycin (0.5 μM, Complex V inhibitor), carbonyl cyanide-4 (trifluoromethoxy) phenylhydrazone (FCCP; 1 μM, oxidative phosphorylation uncoupler), and a rotenone-antimycin A mix (0.5 μM, Complex I and III inhibitors) were injected sequentially to interrogate mitochondrial function. Parameters of this test were calculated according to the manufacturer's instructions.

### 2.11.2 | Glycolysis stress test

This test was run in accordance with the manufacturer's instructions (catalog number 103020-100, Agilent, UK). Following the initial baseline reads, sequential injections of 10 mM glucose (supraphysiological concentration to saturate the cells with glucose), 1 μM oligomycin, and 50 mM 2DG were used to interrogate the glycolytic capabilities of the cells. Parameters of this test were calculated according to the manufacturer's instructions, substituting rates post-2DG for pre-glucose injection rates as a measure of non-glycolytic metabolism.

### 2.11.3 | Fatty acid oxidation stress test

Cells were plated 48 h prior to the assay. 24 h before the assay, plating media was replaced with substrate-limited media (DMEM [catalog number 11966, Fisher Scientific UK]; 0.5 mM glucose, 1 mM glutamate, 0.5 mM carnitine, 1% FBS) overnight. Carnitine supplementation was used to promote fatty acid oxidation (FAO). 45 minutes prior to the assay, substrate-limited media was replaced with

fatty acid oxidation media (111 mM NaCl, 4.7 mM KCl, 1.25 mM $CaCl_2$, 2 mM $MgSO_4$, 1.2 mM $NaH_2PO_4$, 2.5 mM glucose, 0.5 mM carnitine, and 5 mM HEPES, pH 7.4). 45 minutes into the degas period, half the cells were treated with 40 μM etomoxir (catalog number E1905-5MG, Merck Millipore UK), an inhibitor of CPT1 function. This concentration was chosen to avoid off-target effects associated with higher concentrations of etomoxir (Divakaruni et al., 2018). Immediately before running the assay, half of the etomoxir and control treated cells were treated with 200 μM palmitate (catalog number P0500, Merck Millipore, UK) or bovine serum albumin (BSA) vehicle (0.17 mM; catalog number 10775835001, Merck Millipore, UK). A mitochondrial stress test (described above) was then performed to assess mitochondrial fatty acid oxidation. Basal FAO was calculated as the difference in oxygen consumption rate (OCR) between cells co-treated with palmitate and etomoxir, and cells treated with palmitate alone, immediately before oligomycin was injected. Maximal FAO was calculated as the difference in OCR between cells co-treated with palmitate and etomoxir, and cells treated with palmitate alone, at the highest rate measurement following FCCP injection.

### 2.12 | Measurement of extracellular L-lactate

For the assay, $2.1 \times 10^5$ cells were seeded in 6 well dishes 20–24 h prior to experimentation. Following treatments, extracellular L-lactate levels were determined using the L-lactate Assay Kit (catalog number 700510, Cayman Chemical, USA) according to the manufacturer's specifications. Data are expressed as μM lactate/mL media.

### 2.13 | Quantification of cytokine secretion

Following treatments, media samples were collected and centrifuged at 21 000×*g* for 5 min (4°C). 1 volume of sample was diluted in 1 volume of assay media and stored at −70°C. Tumor necrosis factor (TNF) was quantified using a DuoSet ELISA kit (catalog number DY410-05, R&D Systems, UK) according to the manufacturer's instructions.

### 2.14 | Cell viability assay

Cell viability was estimated using a propidium iodide stain (2 μg/mL; catalog number P4864, Merck Millipore [UK]) as previously published (Robb et al., 2020).

### 2.15 | Data analysis

No sample calculations were performed prior to commencing this study. Where feasible, our sample sizes were based on initial data generated using U373 cells. In the event that we did not generate initial data using U373 cells, our sample sizes were informed by our recent study of a similar nature (Robb et al., 2020) or by previous studies in the literature of a similar nature (Tu et al., 2016). Microscope images were processed using FIJI (Fiji Is Just ImageJ (Schindelin et al., 2012); RRID:SCR_002285). Raw data were processed using Microsoft Excel and statistical analyses were performed using GraphPad Prism (v10.0.2 for Windows; GraphPad Software, Boston, MA, USA) (RRID:SCR_002798). Extracellular flux analysis data were normalized to protein content per well using Wave Analysis Software (Agilent; RRID:SCR_024491) and exported to Prism. For each data set, outliers were identified via the robust regression and outlier removal (ROUT) method (Q = 1%). Outliers were removed from the dataset, and normality of data was then assessed using a D'Agostino & Pearson omnibus normality test (alpha = 0.05). If data were non-parametric, a non-parametric statistical test (i.e., Mann–Whitney test or Kruskal–Wallis test) was used. Parametric datasets were analyzed using appropriate parametric statistical tests (i.e., an unpaired two-tailed *t*-test or one-way ANOVA). Data are displayed as mean ± standard error of the mean. A result was deemed to be statistically significant if $p < 0.05$. *p*-values presented in the main body of text have been rounded to two significant figures. Full statistical reports without rounding (df, *F*-values, *t*-values, *p*-values) can be found in the respective figure legends.

## 3 | RESULTS

### 3.1 | TSPO deficiency reduced mitochondrial and non-mitochondrial respiration in mouse primary astrocytes and U373 astrocytoma cells

To characterize the impact of TSPO deficiency on the metabolism of MPAs and astrocytoma cells, $TSPO^{-/-}$ MPAs and U373 cells were examined using extracellular flux analysis (Figure 1). Based on published literature, we hypothesized that TSPO deficiency would reduce basal mitochondrial and glycolytic metabolism in these cells (Tu et al., 2016; Yao et al., 2020). Mean basal oxygen consumption rate (OCR; a proxy of mitochondrial metabolism (Takahashi & Yamaoka, 2017)) was reduced by 31.1% in $TSPO^{-/-}$ MPAs compared to $TSPO^{+/+}$ MPA controls (Figure 1a,b; $p < 0.0001$). Similarly, mean basal extracellular acidification rate (ECAR; a proxy of glycolysis (Mookerjee et al., 2015; Mookerjee & Brand, 2015)) was reduced by 38.8% (Figure 1c,d; $p < 0.0001$). This led us to infer that under basal conditions $TSPO^{-/-}$ MPAs showed reductions in aerobic glycolysis, and oxidative phosphorylation of its products, compared to $TSPO^{+/+}$ counterparts. These results were replicated in $TSPO^{-/-}$ U373 cells, where mean basal OCR was reduced by 15.7% (Figure 1e,f; $p = 0.0293$) and mean basal ECAR was reduced by 45.6% compared to $TSPO^{+/+}$ EV controls (Figure 1g,h; $p < 0.0001$). Together, these data suggest that TSPO deficiency reduces the basal metabolic rates of both MPAs and U373 astrocytoma cells under basal conditions.

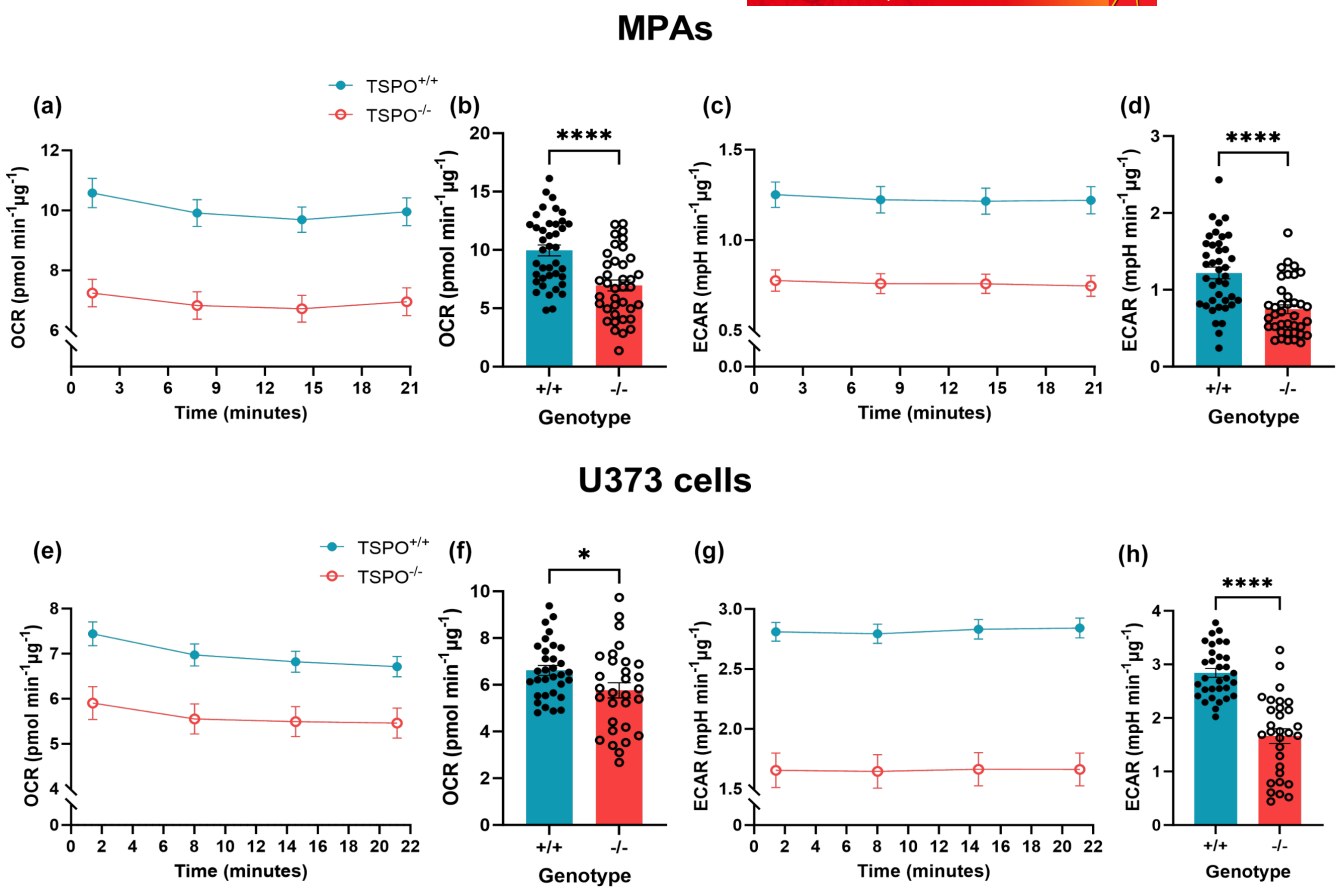


FIGURE 1 TSPO deficiency attenuated basal metabolism in U373 cells and mouse primary astrocytes. (a) Oxygen consumption rate (OCR) of TSPO-deficient ($TSPO^{-/-}$) MPAs compared to wildtype ($TSPO^{+/+}$) controls under basal conditions. (b) Quantification of (a), readings were taken from time point 4 of (a). Unpaired two-tailed *t*-test, df = 76, $t = 4.571$, $p < 0.0001$. (c) Extracellular acidification rate (ECAR) of $TSPO^{-/-}$ MPAs under basal conditions. (d) Quantification of (c), readings were taken from time point 4 of (c). Unpaired two-tailed *t*-test, df = 76, $t = 4.969$, $p < 0.0001$. (a–d) $n = 38–40$ wells, data are pooled from across three independent plates. (e) OCR of $TSPO^{-/-}$ U373 cells compared to empty vector $TSPO^{+/+}$ controls under basal conditions. (f) Quantification of (e), readings were taken from time point 4 of (e). Unpaired two-tailed *t*-test, df = 60, $t = 2.233$, $p = 0.0293$. (g) ECAR of $TSPO^{-/-}$ U373 cells compared to empty vector $TSPO^{+/+}$ controls under basal conditions. (h) Quantification of (g), readings were taken from time point 4 of (g). Unpaired two-tailed *t*-test, df = 60, $t = 7.467$, $p < 0.0001$. (e–h) $n = 30–32$ wells, data are pooled from across three independent plates. $^{*}p < 0.05$, $^{****}p < 0.0001$. Data are expressed as mean ± standard error of the mean.

### 3.2 | TSPO deficiency attenuated the metabolic response to glucopenia

Once basal metabolic profiles of $TSPO^{-/-}$ astrocyte and astrocytoma models had been determined, we used the mitochondrial and glycolysis stress test paradigms to test the metabolic response to energetic stress in these cells, including the ability to switch to alternative substrates when glucose was limited.

We began by assessing changes to mitochondrial metabolism using the mitochondrial stress test (see Figure 2a [MPAs], H [U373s]). We found that, in line with our initial data, basal mitochondrial respiration was significantly reduced in $TSPO^{-/-}$ MPAs (Figure 2b, $p = 0.0006$). This was accompanied by a reduction in mean maximal mitochondrial respiration of 40.2% compared to $TSPO^{+/+}$ MPA controls (Figure 2c, $p = 0.0012$). In $TSPO^{-/-}$ MPAs mitochondria-linked ATP production was reduced by 35.8% (Figure 2d, $p = 0.0009$), and mean proton leak was reduced by 46.0% (Figure 2e, $p < 0.0001$). Coupling efficiency was increased by 2.3% (Figure 2f, $p = 0.0007$), however mitochondrial spare capacity was reduced by 49.3% (Figure 2g, $p = 0.029$). These results were mirrored in $TSPO^{-/-}$ U373 cells (Figure 2h), where mean maximal respiration was reduced by 26.1% compared to $TSPO^{+/+}$ EV controls (Figure 2i, $p = 0.0002$ [basal]; Figure 2j, $p = 0.001$ [maximal]). Mitochondria-linked ATP production was reduced by 26.9% (Figure 2k, $p = 0.0004$) and mean proton leak was reduced by 19.1% (Figure 2l, $p = 0.0011$). However, there was no significant difference in mean coupling efficiency (Figure 2m, $p = 0.17$) in $TSPO^{-/-}$ U373 cells compared to $TSPO^{+/+}$ EV controls, whereas mean spare capacity was reduced by 27.3% (Figure 2n, $p = 0.0025$). Though we were not directly comparing U373 cells to MPAs, considering the divergence of results observed in the mitochondrial stress test we hypothesized that these cells would have different basal bioenergetic profiles. Using extracellular flux analysis, we assessed this experimentally and found that under basal conditions U373 cells showed increased ECAR (a proxy of

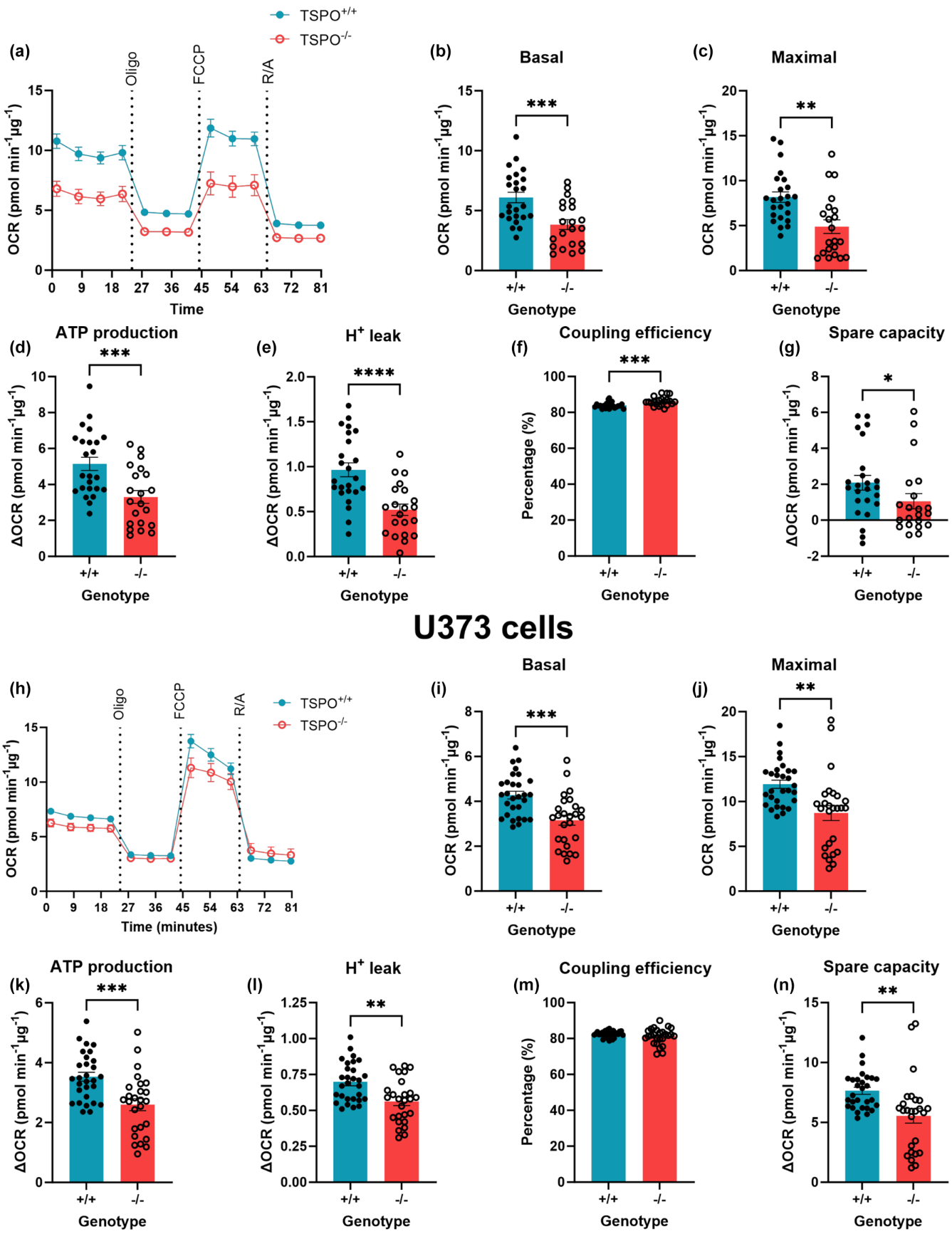

**FIGURE 2** Mitochondrial respiration of astrocytes was reduced by TSPO deficiency. (a) Oxygen consumption rate (OCR) of TSPO-deficient ($TSPO^{-/-}$) MPAs compared to wildtype ($TSPO^{+/+}$) controls during the mitochondrial stress test. Oligo = 0.5 μM oligomycin, FCCP = 1 μM carbonyl cyanide-p-trifluoromethoxyphenylhydrazone, R/A = 0.5 μM rotenone/antimycin A. (b) Basal mitochondrial respiration of $TSPO^{-/-}$ MPAs compared to $TSPO^{+/+}$ controls (difference in OCR prior to oligo injection and following R/A injection). Unpaired two-tailed *t*-test, df = 43, $t = 3.719$, $p = 0.0006$. (c) Maximal mitochondrial respiration of $TSPO^{-/-}$ MPAs compared to $TSPO^{+/+}$ controls (difference in OCR following FCCP injection and after R/A injection). Unpaired two-tailed *t*-test, df = 43, $t = 3.480$, $p = 0.0012$. (d) Mitochondria-linked ATP production of $TSPO^{-/-}$ MPAs compared to $TSPO^{+/+}$ controls (difference in OCR prior to and following oligo injection). Unpaired two-tailed *t*-test, df = 43, $t = 3.567$, $p = 0.0009$. (e) Proton ($H^+$) leak of $TSPO^{-/-}$ MPAs compared to $TSPO^{+/+}$ controls (difference in OCR after FCCP injection and R/A injection). Unpaired two-tailed *t*-test, df = 43, $t = 4.351$, $p < 0.0001$. (f) Coupling efficiency of $TSPO^{-/-}$ MPAs compared to $TSPO^{+/+}$ controls (percentage of (b) used for ATP production). Mann–Whitney test, $p = 0.0007$. (g) Mitochondrial spare capacity of $TSPO^{-/-}$ MPAs compared to $TSPO^{+/+}$ controls (difference in OCR between (b) and (c)). Mann–Whitney test, $p = 0.0292$. (a–g) $n = 21$–24 wells per genotype, data are pooled from across three separate plates. (h) Oxygen consumption rate (OCR) of $TSPO^{-/-}$ U373 cells compared to empty vector (EV) $TSPO^{+/+}$ controls during the mitochondrial stress test. Oligo = 0.5 μM oligomycin, FCCP = 1 μM carbonyl cyanide-p-trifluoromethoxyphenylhydrazone, R/A = 0.5 μM rotenone/antimycin A. (i) Basal mitochondrial respiration of $TSPO^{-/-}$ U373 cells compared to EV $TSPO^{+/+}$ controls. Unpaired two-tailed *t*-test, df = 53, $t = 3.9261$, $p = 0.0002$. (j) Maximal mitochondrial respiration of $TSPO^{-/-}$ U373 cells compared to EV $TSPO^{+/+}$ controls. Unpaired two-tailed *t*-test, df = 53, $t = 3.477$, $p = 0.0010$. (k) Mitochondria-linked ATP production of $TSPO^{-/-}$ U373 cells compared to EV $TSPO^{+/+}$ controls. Unpaired two-tailed *t*-test, df = 53, $t = 3.793$, $p = 0.0004$. (l) Proton ($H^+$) leak of $TSPO^{-/-}$ U373 cells compared to EV $TSPO^{+/+}$ controls. Unpaired two-tailed *t*-test, df = 53, $t = 3.453$, $p = 0.0011$. (m) Coupling efficiency of $TSPO^{-/-}$ U373 cells compared to EV $TSPO^{+/+}$ controls (percentage of (i) used for ATP production). Unpaired two-tailed *t*-test, df = 53, $t = 1.376$, $p = 0.1747$. (n) Mitochondrial spare capacity of $TSPO^{-/-}$ U373 cells compared to EV $TSPO^{+/+}$ controls (difference between (i) and (j)). Unpaired two-tailed *t*-test, df = 53, $t = 3.175$, $p = 0.0025$. (i–n) $n = 26$–29 wells per genotype, data are pooled from across three separate plates. $^*p < 0.05$, $^{**}p < 0.01$, $^{***}p < 0.001$, $^{****}p < 0.0001$. Data are expressed as mean ± standard error of the mean.

glycolysis) and reduced OCR (a proxy of mitochondrial respiration) relative to MPAs, therefore we propose that variations in the bioenergetic parameters between $TSPO^{-/-}$ MPAs and U373 cells may be accounted for by these differences in basal bioenergetic profiles (Figure S4).

Next, we examined the effect of TSPO deficiency on glycolysis in MPA and U373 cells via the glycolysis stress test (Figure 3a [MPAs], 3f [U373s]). In this paradigm, a glucose-free incubation period (glucopenia) followed by glucose injection is used to examine the glycolytic rate of the cells. Because our previous data (Figures 1 and 2) showed that both $TSPO^{-/-}$ MPAs and U373s had reduced ECAR compared to their respective $TSPO^{+/+}$ controls, we hypothesized that TSPO deficiency in these cells results in reduced glycolysis. Notably, we found that non-glycolytic acidification—acidification of the media that may be attributed to other cellular or metabolic processes that produce $H^+$, such as FAO (Muthuramu et al., 2015)—was significantly increased in $TSPO^{-/-}$ MPAs (Figure 3b, $p < 0.0001$) and $TSPO^{-/-}$ U373s (Figure 3g, $p = 0.0057$). Meanwhile, in contrast to our hypothesis (that TSPO deficiency would reduce glycolysis), we found that mean glycolytic rate was increased by 18.0% in $TSPO^{-/-}$ MPAs (Figure 3c, $p < 0.0001$). Similarly, mean glycolytic capacity and reserve were increased by 25.8% and 27.6%, respectively (Figure 3d,e; $p < 0.0001$ [both parameters]). In $TSPO^{-/-}$ U373 cells, the mean glycolytic rate was reduced by 26.5% (Figure 3h, $p < 0.0001$) and we observed no change in glycolytic capacity in $TSPO^{-/-}$ U373 cells compared to $TSPO^{+/+}$ EV controls (Figure 3i, $p = 0.38$). However, mean glycolytic reserve was increased by 72.9% in $TSPO^{-/-}$ U373 cells (Figure 3j, $p < 0.0001$).

We were particularly intrigued by the apparently contradictory nature of our results in $TSPO^{-/-}$ MPAs—whereas our initial data showed that a proxy of glycolysis (ECAR) was reduced in $TSPO^{-/-}$ MPAs in the presence of glucose (Figures 1 and 2), our data from the glycolysis stress test (Figure 3) showed a relative increase in glycolytic metabolism in these cells, including basal ECAR prior to the injection of glucose (non-glycolytic acidification, Figure 3b, $p < 0.0001$). Postulating that this may have arisen due to a difference in the experimental protocol—namely, the period of glucose starvation followed by the reintroduction of glucose inherent to the glycolysis stress test paradigm, compared to consistent glucose availability in the mitochondrial stress test—we hypothesized that TSPO deficiency may alter the metabolic adaptations when glucose is absent (glucopenia). We tested this by comparing on the same plate the initial conditions of the mitochondrial stress test (glucose present throughout) and glycolysis stress test (glucose absent initially): incubating $TSPO^{-/-}$ and $TSPO^{+/+}$ MPAs either in the presence or absence of glucose to directly compare their basal metabolic rates under these different conditions (Figure 4a–d). Using a two-way ANOVA we observed no statistically significant effects of genotype on OCR (Figure 4a,c; $p_{genotype} = 0.64$, $F_{(1,58)} = 0.2246$) and ECAR (Figure 4b,d; $p_{genotype} = 0.16$, $F_{(1,58)} = 1.987$). However, we observed a statistically significant impact of glucose concentration on OCR (Figure 4a,c; $p_{glucose} = 0.044$, $F_{(1,58)} = 4.232$) and ECAR (Figure 4a,d; $p_{glucose} = 0.035$, $F_{(1,58)} = 4.654$), and a statistically significant interaction of these variables on OCR ($p_{interaction} = 0.0034$, $F_{(1,58)} = 9.348$) and ECAR ($p_{interaction} = 0.019$, $F_{(1,58)} = 5.186$). Post-hoc analyses revealed that, under glucose-free conditions, mean basal OCR and ECAR of $TSPO^{+/+}$ MPAs were reduced by 33.9% and 43.9% respectively compared to when glucose was present (Figure 4a–d; $p = 0.0031$ [OCR], $p = 0.0103$ [ECAR]). Although the basal OCR and ECAR of $TSPO^{-/-}$ MPAs were lower than $TSPO^{+/+}$ MPAs they did not change in the absence of glucose (Figure 4a–d; $p = 0.9823$ [OCR], $p > 0.9999$ [ECAR]) suggesting that $TSPO^{-/-}$ MPAs may be less dependent on glucose to maintain their basal metabolic rate than their $TSPO^{+/+}$ controls.

To confirm the results of our extracellular flux analyses (Figure 4a–d), we quantified the secretion of L-lactate from

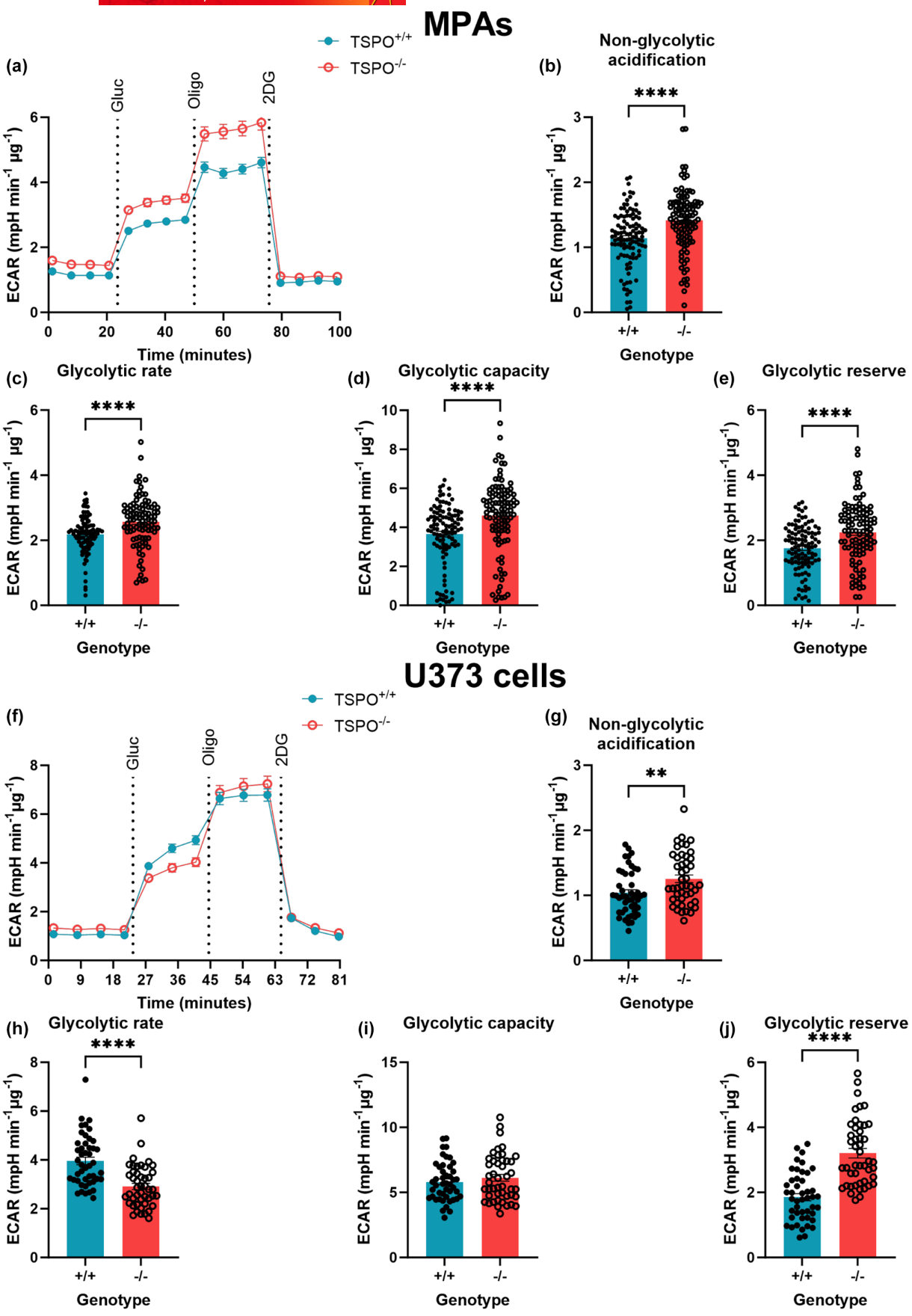

**FIGURE 3** TSPO deficiency increased glycolytic rate in MPAs but reduced glycolytic rate in U373 astrocytoma cells. (a) Extracellular acidification rate (ECAR) of TSPO-deficient ($TSPO^{-/-}$) MPAs compared to wildtype ($TSPO^{+/+}$) controls during the glycolysis stress test. Gluc = 10 mM glucose, oligo = 1 μM oligomycin, 2DG = 50 mM 2-deoxyglucose. (b) Non-glycolytic acidification of $TSPO^{-/-}$ MPAs compared to $TSPO^{+/+}$ controls (ECAR immediately prior to glucose injection). Unpaired two-tailed *t*-test, df = 211, $t = 4.549$, $p < 0.0001$. (c) Glycolytic rate of $TSPO^{-/-}$ MPAs compared to $TSPO^{+/+}$ controls (ECAR after glucose injection immediately prior to oligo injection). Mann–Whitney test, $p < 0.0001$. (d) Glycolytic capacity of $TSPO^{-/-}$ MPAs compared to $TSPO^{+/+}$ controls (difference between maximum ECAR after oligo injection and non-glycolytic acidification). Mann–Whitney test, $p < 0.0001$. (e) Glycolytic reserve of $TSPO^{-/-}$ MPAs compared to $TSPO^{+/+}$ controls (difference between glycolytic rate and capacity). Unpaired two-tailed *t*-test, df = 210, $t = 4.313$, $p < 0.0001$. (a–e) $n = 105$–108 wells, data are pooled from across three independent plates. (f) ECAR of $TSPO^{-/-}$ U373 cells compared to empty vector (EV) $TSPO^{+/+}$ controls during the glycolysis stress test. Gluc = 10 mM glucose, oligo = 1 μM oligomycin, 2DG = 50 mM 2-deoxyglucose. (g) Non-glycolytic acidification of $TSPO^{-/-}$ U373 cells compared to EV $TSPO^{+/+}$ controls. Unpaired two-tailed *t*-test, df = 90, $t = 2.835$, $p = 0.0057$. (h) Glycolytic rate of $TSPO^{-/-}$ U373 cells compared to EV $TSPO^{+/+}$ controls. Mann–Whitney test, $p < 0.0001$. (i) Glycolytic capacity of $TSPO^{-/-}$ U373 cells compared to EV $TSPO^{+/+}$ controls. Unpaired two-tailed *t*-test, df = 90, $t = 0.8868$, $p = 0.3776$. (j) Glycolytic reserve of $TSPO^{-/-}$ U373 cells compared to EV $TSPO^{+/+}$ controls. Unpaired two-tailed *t*-test, df = 90, $t = 7.346$, $p < 0.0001$. (f–j) $n = 46$ wells, data are pooled from across three independent plates. $^{**}p < 0.01$, $^{****}p < 0.0001$. Data are expressed as mean ± standard error of the mean.

$TSPO^{-/-}$ and wildtype control MPA and U373 astrocytoma cells as a secondary experimental measure of glycolysis (Figure 4e,f). As the conjugate base of lactic acid, L-lactate would acidify media if secreted from the cells, resulting in the changes in ECAR observed in our metabolic flux assays. In MPAs, TSPO genotype had a statistically significant effect on L-lactate secretion (Figure 4e, $p_{genotype} = 0.0011$, $F_{(1,20)} = 14.55$), as did glucose concentration ($p_{genotype} < 0.0001$, $F_{(1,20)} = 25.04$). We observed a statistically significant interaction of these variables in MPAs ($p_{genotype} = 0.032$, $F_{(1,20)} = 5.298$). Post-hoc analysis revealed that in the presence of glucose $TSPO^{-/-}$ MPAs secreted 5.6% less L-lactate than $TSPO^{+/+}$ controls (Figure 4e, $p = 0.002$). In the absence of glucose, while $TSPO^{+/+}$ MPAs reduced their L-lactate secretion by 6.7% (Figure 4e, $p = 0.0003$), L-lactate secretion was not altered in $TSPO^{-/-}$ MPAs (Figure 4e, $p = 0.35$). In U373 astrocytoma cells, TSPO genotype did not have a statistically significant effect on L-lactate secretion (Figure 4f, $p_{genotype} = 0.20$, $F_{(1,20)} = 1.748$), however we observed a statistically significant effect of glucose concentration on L-lactate secretion from these cells ($p_{glucose} = 0.0015$, $F_{(1,20)} = 7.159$). Moreover, we observed a statistically significant interaction between these variables ($p_{interaction} = 0.0001$, $F_{(1,20)} = 21.84$). Post-hoc analyses of this data supported our results from MPAs: mean L-lactate secretion was reduced by 20.4% in $TSPO^{-/-}$ U373 cells compared to $TSPO^{+/+}$ EV controls (Figure 4f, $p = 0.0024$) under basal conditions. Further, unlike $TSPO^{+/+}$ EV controls, which altered their L-lactate secretion in response to glucopenia (Figure 4f, $p = 0.0003$), L-lactate secretion from $TSPO^{-/-}$ U373 cells was unchanged under glucopenic conditions (Figure 4f, $p = 0.68$). Thus, when considered together, our data from MPAs and U373 astrocytoma cells supports the notion that TSPO deficiency in these cells makes them less reliant on glucose to maintain their metabolic requirements in the absence of glucose and recapitulates the data we obtained from MPAs using the metabolic flux analyses (Figure 4a–d). When considered with our metabolic flux analyses (Figure 4a–d), these data suggest that, compared to $TSPO^{+/+}$ controls, $TSPO^{-/-}$ deficient MPAs and U373 cells may be meeting their bioenergetic requirements by preferentially metabolizing substrates other than glucose.

### 3.3 | $TSPO^{-/-}$ mouse primary astrocytes and U373 cells used fatty acid oxidation to maintain their metabolic rate

As we observed that $TSPO^{-/-}$ MPA and U373 cells were able to maintain their metabolic parameters (albeit at a lower bioenergetic rate) in the absence of glucose (Figure 4a–d), and produced less L-lactate under basal conditions (Figure 4e,f), we postulated that in the context of TSPO deficiency these cells can more readily utilize other metabolic substrates.

In MA-10 Leydig cells, which like astrocytes are capable of fatty acid metabolism and steroidogenesis, TSPO deficiency can increase fatty acid oxidation (FAO) and overexpression of TSPO is linked to reduced expression of genes involved with FAO (Tu et al., 2016). Hence, we hypothesized that $TSPO^{-/-}$ MPAs and U373 cells were meeting their bioenergetic requirements through enhanced fatty acid metabolism and postulated that this might explain their enhanced non-glycolytic acidification (Figure 3b,g). We used a fatty acid oxidation stress test (FAOST) to examine the contribution of FAO to maintaining $TSPO^{-/-}$ MPA and U373 metabolism (Figure 5a [MPAs], 5d [U373s]). This assay involves an overnight incubation in limited glucose media (0.5 mM) supplemented with carnitine (0.5 mM) to promote FAO. During the assay, half the cells are treated with palmitate (C16; a saturated fatty acid) to induce FAO, and half of the C16- and control-treated cells are also treated with etomoxir, an inhibitor of CPT1a, the rate-limiting enzyme of FAO. This allows the contribution of FAO to maintaining the basal metabolic rates of the cells to be assessed. By sequentially injecting the same compounds used in the mitochondrial stress test paradigm (oligomycin [0.5 μM], FCCP [1 μM], rotenone-antimycin A [0.5 μM]), we were able to calculate 'maximal' FAO, an estimation of the extent to which cells use FAO to resolve metabolic stress.

We found that mean basal FAO was increased by 241.0% in $TSPO^{-/-}$ MPAs (Figure 5b, $p = 0.031$) compared with $TSPO^{+/+}$ MPAs. This suggests that lipids constituted a greater proportion of the substrates used to maintain basal metabolic rates in $TSPO^{-/-}$ MPAs compared with $TSPO^{+/+}$ MPAs. Similarly, maximal FAO was enhanced in $TSPO^{-/-}$ MPAs (Figure 5c, $p = 0.0004$). In $TSPO^{-/-}$ U373 cells, we did not see any change in basal FAO (Figure 5e, $p = 0.28$), however mean maximal FAO was increased by 245.5%

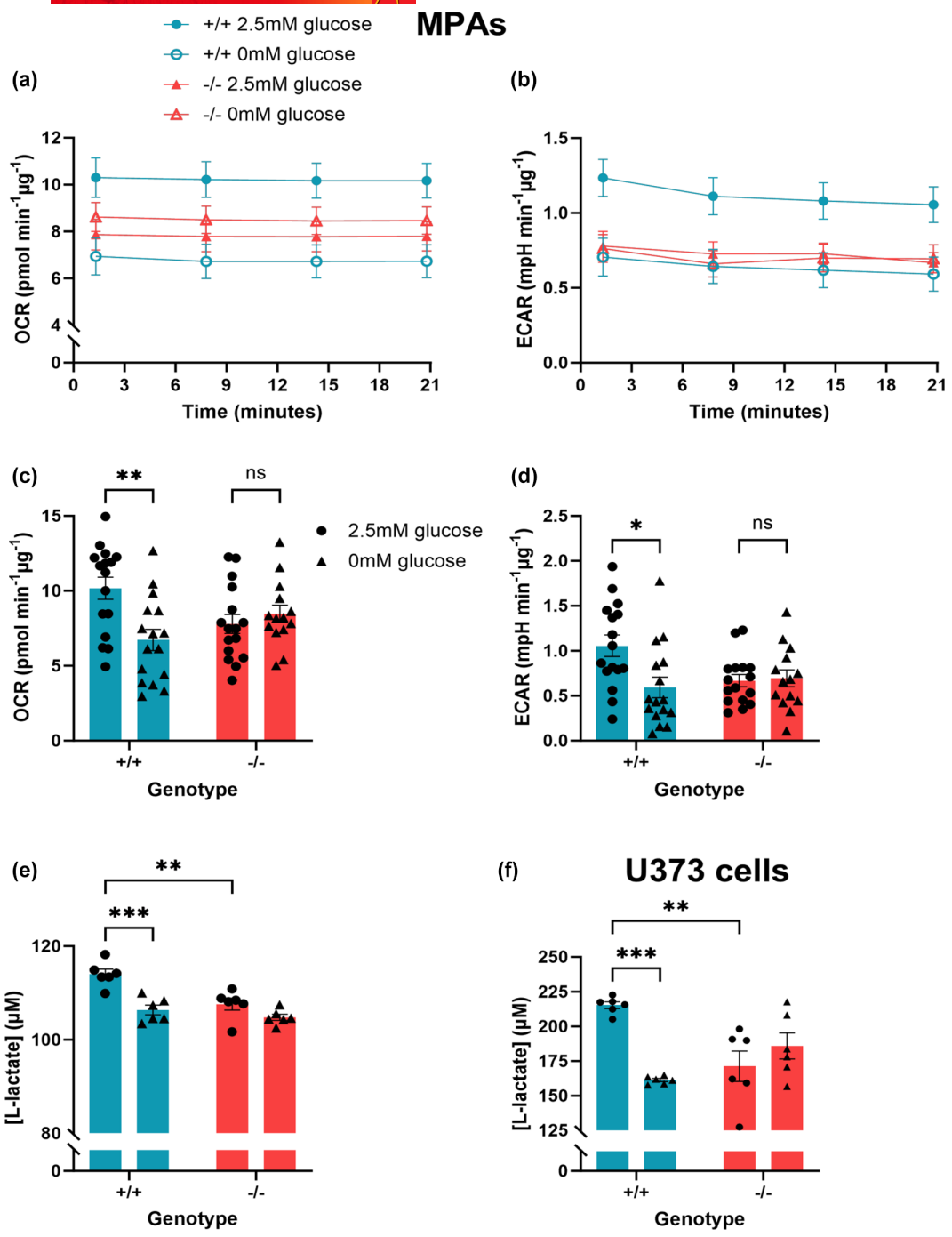


FIGURE 4 TSPO$^{-/-}$ astrocytes secreted less L-lactate in the presence of glucose and lactate secretion was not affected by glucopenia. (a) Oxygen consumption rate (OCR) of TSPO-deficient (TSPO$^{-/-}$) MPAs ± glucose (2.5 mM) compared to wildtype (TSPO$^{+/+}$) controls ± glucose. (b) Extracellular acidification rate (ECAR) of TSPO$^{-/-}$ MPAs ± glucose compared to TSPO$^{+/+}$ controls ± glucose. (c) Quantification of (a) at time point 4. 2-way ANOVA with Šídák's multiple comparisons test, $p_{genotype}=0.6373$, $F_{(1,58)}=0.2246$. $p_{glucose}=0.0442$, $F_{(1,58)}=4.232$. $p_{interaction}=0.0034$, $F_{(1,58)}=9.348$. (d) Quantification of (b) at time point 4. 2-way ANOVA with Šídák's multiple comparisons test, $p_{genotype}=0.1640$, $F_{(1,58)}=1.987$. $p_{glucose}=0.0351$, $F_{(1,58)}=4.654$. $p_{interaction}=0.0191$, $F_{(1,58)}=5.186$. (e) Extracellular L-lactate concentrations sampled from TSPO$^{-/-}$ MPAs ± glucose and TSPO$^{+/+}$ controls ± glucose. 2-way ANOVA with Šídák's multiple comparisons test, $p_{genotype}=0.0011$, $F_{(1,20)}=14.55$. $p_{glucose}<0.0001$, $F_{(1,20)}=25.04$. $p_{interaction}=0.0322$, $F_{(1,20)}=5.298$. (f) Extracellular L-lactate concentrations sampled from TSPO$^{-/-}$ U373 cells ± glucose and empty vector TSPO$^{+/+}$ controls ± glucose. 2-way ANOVA with Šídák's multiple comparisons test, $p_{genotype}=0.2011$, $F_{(1,20)}=1.748$. $p_{glucose}=0.00145$, $F_{(1,20)}=7.159$. $p_{interaction}=0.0001$, $F_{(1,20)}=21.84$. (a–d) $n=14$–16 wells from one plate to directly examine trends in basal metabolism observed in Figures 1–3. (e, f) $n=6$ wells. ns $p>0.05$, *$p<0.05$, **$p<0.01$, ***$p<0.001$. Data are expressed as mean ± standard error of the mean.

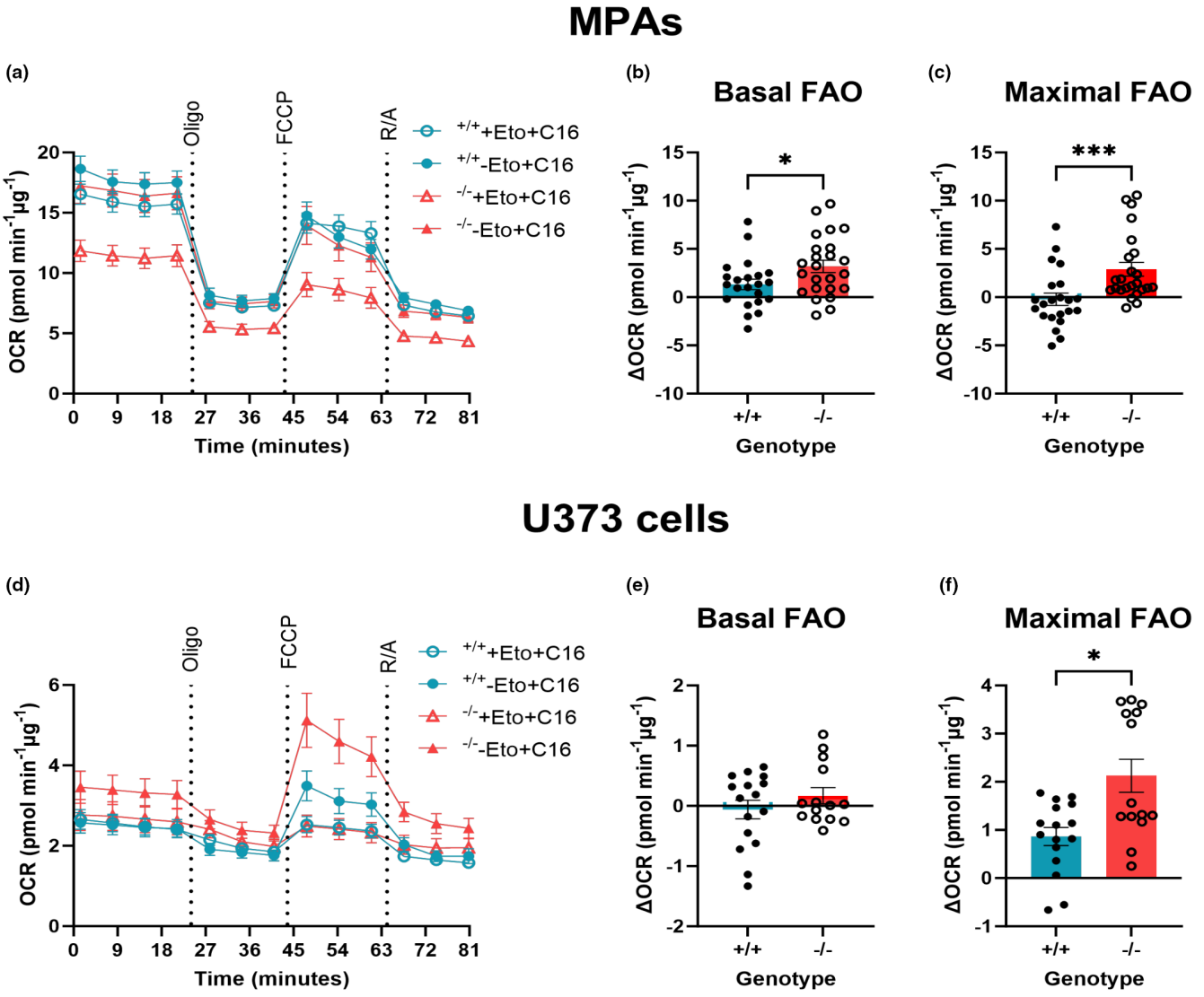


FIGURE 5 Basal fatty acid oxidation was enhanced in TSPO$^{-/-}$ MPAs. (a) Oxygen consumption rate (OCR) of TSPO-deficient (TSPO$^{-/-}$) MPAs compared to wildtype (TSPO$^{+/+}$) controls during the fatty acid oxidation stress test. 15 min prior to the test, 50% of cells were treated with etomoxir (Eto; 40 µM). 50% of cells were treated with palmitate (C16; 200 µM) or bovine serum albumin vehicle (BSA; 0.17 mM) immediately prior to the test. Oligo = 0.5 µM oligomycin, FCCP = 1 µM carbonyl cyanide-p-trifluoromethoxyphenylhydrazone, R/A = 0.5 µM rotenone/antimycin A. (b) Basal fatty acid oxidation (FAO) of TSPO$^{-/-}$ MPAs compared to TSPO$^{+/+}$ controls (difference between etomoxir-treated and comparable controls immediately prior to oligo injection). Unpaired two-tailed *t*-test, df = 44, $t = 2.231$, $p = 0.0308$. (c) Maximal FAO of TSPO$^{-/-}$ MPAs compared to TSPO$^{+/+}$ controls (difference between etomoxir-treated and comparable controls after FCCP injection). Mann–Whitney test, $p = 0.0004$. (a–c) $n = 22$–24 wells. Data are pooled from across two independent plates. (d) Oxygen consumption rate (OCR) of TSPO$^{-/-}$ (KO) U373 cells compared to empty vector (EV) TSPO$^{+/+}$ controls during the fatty acid oxidation stress test. Oligo = 0.5 µM oligomycin, FCCP = 1 µM carbonyl cyanide-p-trifluoromethoxyphenylhydrazone, R/A = 0.5 µM rotenone/antimycin A. (e) Basal FAO of TSPO$^{-/-}$ U373 cells compared to EV TSPO$^{+/+}$ controls (difference between etomoxir-treated and comparable controls immediately prior to oligo injection). Unpaired two-tailed *t*-test, df = 28, $t = 1.099$, $p = 0.2812$. (f) Maximal FAO of TSPO$^{-/-}$ U373 cells compared to EV TSPO$^{+/+}$ controls (difference between etomoxir-treated and comparable controls after FCCP injection). Mann–Whitney test, $p = 0.0277$. (d–f) $n = 14$–16 wells. Data are pooled from across two independent plates. $^{*}p < 0.05$, $^{***}p < 0.001$. Data are expressed as mean ± standard error of the mean.

(Figure 5f, $p = 0.028$). Together these data suggest that TSPO deficiency increased the contribution of fatty acids as an energy source for MPA metabolism, which may explain how the TSPO$^{-/-}$ MPAs were able to maintain OCR and ECAR in the absence of glucose (Figure 4). The different rates of FAO we observed between U373 astrocytoma cells and MPAs may be due to the relatively increased reliance of MPAs on OCR to meet their bioenergetic requirements (Figure S4).

### 3.4 | TSPO formed a complex with CPT1a in mouse primary astrocytes and U373 cells

Having established that TSPO deficiency modulates FAO in mouse primary astrocytes, we began to explore the potential underlying mechanism. CPT1a, the rate-limiting enzyme of FAO (Houten et al., 2016; Schlaepfer & Joshi, 2020), resides in the outer mitochondrial membrane (Liang, 2023). Previous work has established that CPT1a forms part of a complex with another outer mitochondrial membrane protein, the voltage-dependent anion channel (VDAC) (Lee et al., 2011; Liang, 2023). VDAC is known to form complexes with TSPO (Gatliff et al., 2014), but the existence of a protein complex containing TSPO and CPT1a has not yet been experimentally confirmed. Our data suggesting that TSPO deficiency increases FAO in astrocytes supports a potential role of TSPO in regulating FAO via a protein complex with CPT1a. To address this possibility, we first transiently transfected U373 cells naïve to previous genetic modification with a Myc-DDK tagged TSPO construct. Co-immunoprecipitation was used to identify TSPO-containing complexes via a pulldown using anti-Myc bound agarose beads. Using this method, we established that TSPO is part of a protein complex containing both VDAC and CPT1a (Figure 6a, $n=4$). As this interaction was characterized using transfected cells, to validate this finding we performed a further co-immunoprecipitation using proteins endogenous to U373 cells that were not subject to transfection and determined that this interaction also occurred between endogenous TSPO and CPT1a (Figure 6b,c; $n=3$). Having validated this interaction in U373 cells, and owing to the well-recognized differences between astrocytoma cells and primary astrocytes, we then repeated our experiment presented in Figure 6b,c with MPAs. Having confirmed the specificity of our protocol in Figure 6b,c, we next validated our co-immunoprecipitation in MPAs by using CPT1a and TSPO antibodies to immunoprecipitate CPT1a and TSPO respectively from MPA whole cell lysate (Figure 6d,e; $n=4$). We next tested our hypothesis that TSPO formed part of a protein complex with CPT1a in MPAs by first performing a co-immunoprecipitation on MPA whole cell lysate using a CPT1a antibody, and found that we were able to immunoprecipitate TSPO (Figure 6f; $n=4$). To confirm this interaction, we repeated the co-immunoprecipitation with a TSPO antibody and found that we were able to immunoprecipitate CPT1a (Figure 6g; $n=4$), confirming that TSPO and CPT1a form part of a protein complex in MPAs.

### 3.5 | TSPO expression increased in mouse primary astrocytes after 24 h but not 3 h LPS stimulation, which temporally corresponded to LPS-induced changes in cellular metabolism

TSPO is expressed at a low level under basal conditions throughout the mammalian CNS (Betlazar et al., 2018), with much of this expression being localized to astrocytes (Betlazar et al., 2018; Hernstadt et al., 2009). During various CNS pathologies associated with neuroinflammation, expression of TSPO increases throughout the CNS (Fairley, Wong, & Barron, 2021; Nutma et al., 2021; Shehadeh et al., 2019). Importantly, inflammatory responses are associated with a shift in cellular metabolism linked to increased energy demand (O'Neill et al., 2016; Robb et al., 2019), and we have shown previously that astrocytes undergo a bioenergetic shift to rely more heavily on mitochondrial metabolism after 24 h exposure to inflammatory stimuli (Robb et al., 2020). The data we have presented in Figures 1–6 suggests that TSPO deficiency modulates bioenergetics in MPAs, thus we hypothesized that TSPO expression may increase in astrocytes during inflammation to help meet the increased metabolic demands of inflammatory responses. To test this hypothesis, we treated astrocytes isolated from wildtype C57BL/6J neonates with LPS for 3 h or 24 h, and interrogated changes to TSPO via immunoblotting (Figure 7) and extracellular flux analysis to assess any corresponding metabolic changes (Figure 8). We included the potent

**FIGURE 6** TSPO formed part of a protein complex with CPT1a. (a) Representative immunoblot showing co-immunoprecipitation of a Myc-tagged translocator protein 18 kDa (TSPO) construct (TSPO-Myc) with endogenous carnitine palmitoyltransferase 1a (CPT1a) in U373 cells. U373 cells were transiently transfected with TSPO-Myc plasmids (OriGene), and lysate harvested 24 h later. Co-immunoprecipitations (co-IPs) were performed using Myc-tagged agarose beads (Proteintech). Input (I), unbound fraction (UB) and bound fractions (B) were retained for immunoblotting. Nitrocellulose membranes were blotted for voltage dependent anion channel 1 (VDAC1) (abcam) as a positive control, followed by CPT1a (Proteintech), and Myc (Proteintech) to confirm successful transfection. n = 4 separate immunoprecipitations. (b) Representative immunoblot showing endogenous co-immunoprecipitation of TSPO via CPT1a antibody in cell lysate harvested from U373 cells. Antibody specificity was confirmed using species-specific IgG controls. Whole cell lysate was run as a positive control for protein expression, and supernatant (Lys) or eluate (Elu) from the respective antibody (IgG, TSPO, or CPT1a) incubations were used to confirm successful co-immunoprecipitation. $n=3$ separate immunoprecipitations. (c) Representative immunoblot showing endogenous co-immunoprecipitation of CPT1a via TSPO antibody in cell lysate harvested from U373 cells. Antibody specificity was confirmed using species-specific IgG controls. Whole cell lysate was run as a positive control for protein expression, and Lys or Elu from the respective antibody (IgG, TSPO, or CPT1a) incubations were used to confirm successful co-immunoprecipitation. $n=3$ separate immunoprecipitations. (d) representative immunoblot confirming specificity of endogenous co-immunoprecipitation in MPAs. Immunoprecipitation of CPT1a (CPT1a IP) with nitrocellulose membrane stained for CPT1a (CPT1a immunoblot (IB)). $n=4$ separate immunoprecipitations. (e) representative immunoblot confirming specificity of endogenous co-immunoprecipitation in MPAs. Immunoprecipitation of TSPO (TSPO IP) with nitrocellulose membrane stained for TSPO (TSPO IB). $n=4$ separate immunoprecipitations. (f) Co-IP performed using CPT1a antibody isolated TSPO (CPT1a IP, TSPO IB) in MPA lysate. $n=4$ separate immunoprecipitations. (g) Co-IP performed using TSPO antibody isolated CPT1a (TSPO IP, CPT1a IB) in MPA lysate. $n=4$ separate immunoprecipitations. co-IPs, co-immunoprecipitations; IB, immunoblot; kDa, kilodaltons; L, ladder; MPAs, mouse primary astrocytes.

Journal of Neurochemistry JNC The Official Journal of the International Society for Neurochemistry WILEY



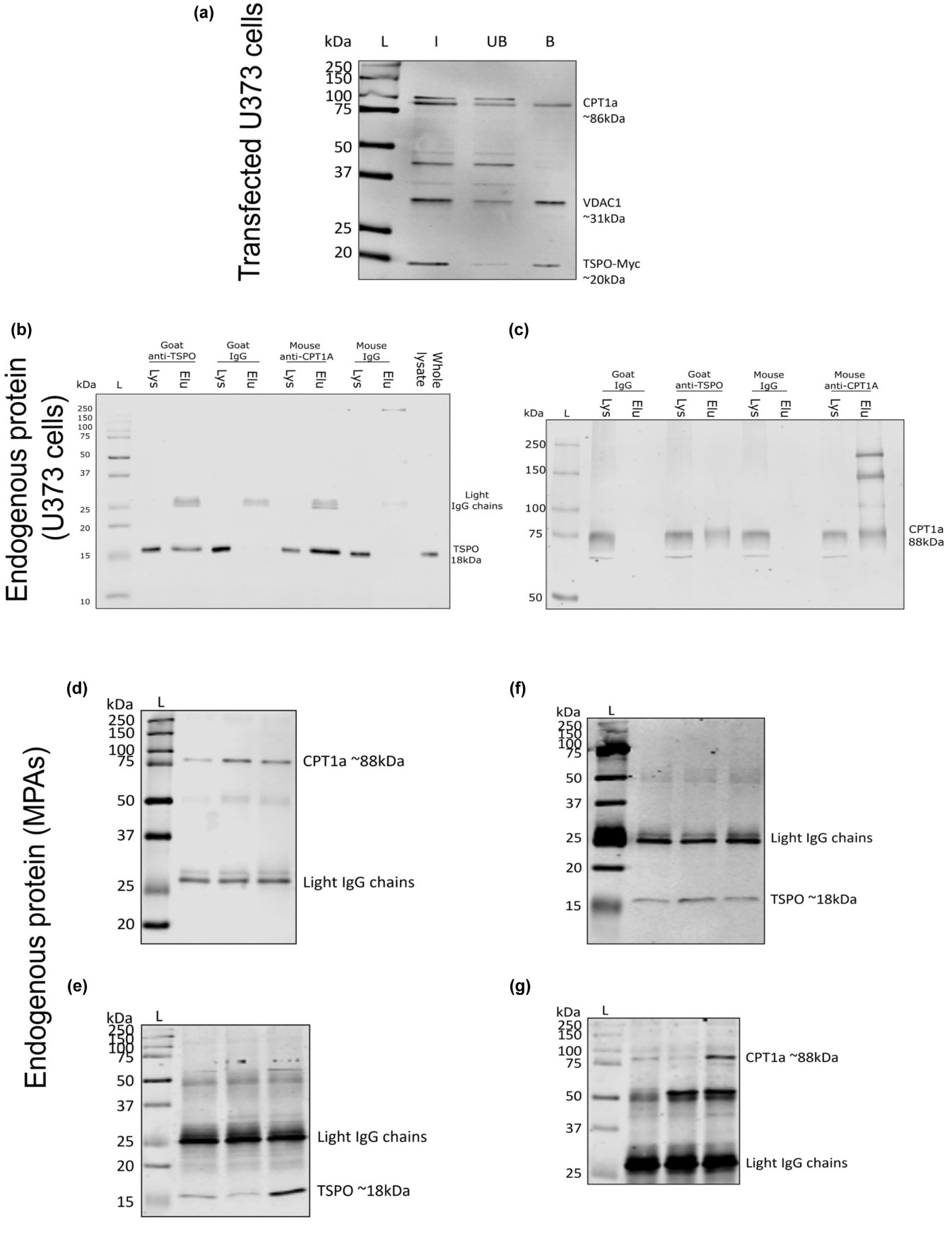

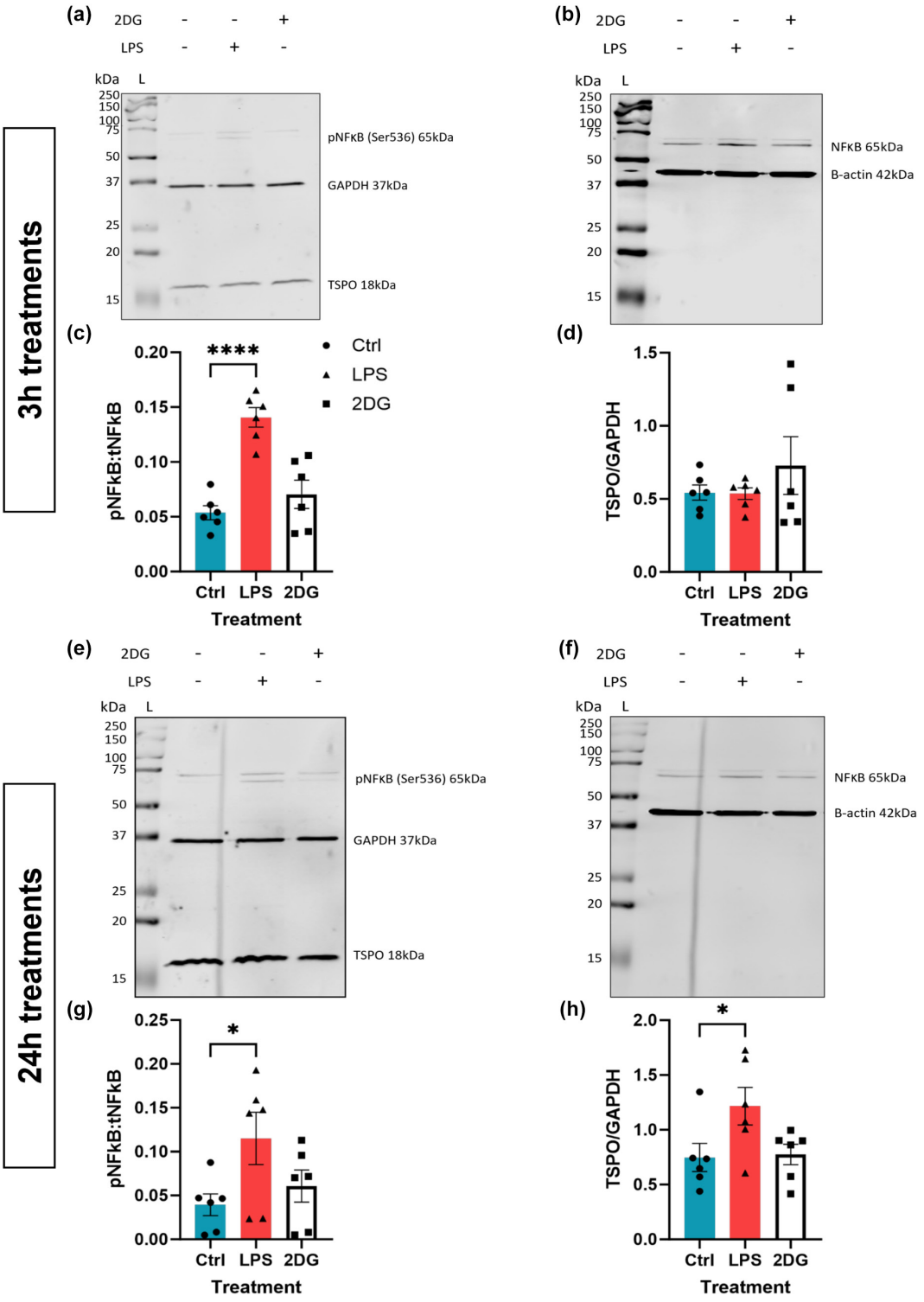


FIGURE 7 24 h but not 3 h LPS stimulation increased TSPO expression in C57BL/6J MPAs. (a, b) Representative immunoblots of C57BL/6J MPA lysate following 3 h stimulation with lipopolysaccharide (LPS; 100 ng/mL) or 2-deoxyglucose (2DG; 10 mM). (a) Representative immunoblot for phosphorylated nuclear factor kappa B (NFκB) p65 (Ser536) (pNFκB), glyceraldehyde phosphate dehydrogenase (GAPDH), and translocator protein (TSPO). (b) Representative immunoblot for total NFκB p65 (tNFκB) and β-actin. (c) Quantification of NFκB activation following 3 h LPS or 2DG stimulation expressed as the ratio of pNFκB:NFκB. One-way ANOVA with Dunnett's multiple comparisons test, $df_{LPS}=15$, $p_{LPS}<0.0001$, $df_{2DG}=15$, $p_{2DG}=0.3910$. (d) Quantification of TSPO expression following 3 h LPS or 2DG stimulation. One-way ANOVA with Dunnett's multiple comparisons test, $df_{LPS}=15$, $p_{LPS}=0.9984$, $df_{2DG}=15$, $p_{2DG}=0.4655$. (e, f) Representative immunoblots of C57BL/6J MPA lysate following 24 h stimulation with LPS or 2DG. (e) Representative immunoblot for pNFκB, GAPDH, and TSPO. (f) Representative immunoblot for tNFκB and β-actin. (g) Quantification of NFκB activation following 24 h LPS or 2DG stimulation expressed as the ratio of pNFκB:NFκB. One-way ANOVA with Dunnett's multiple comparisons test, $df_{LPS}=15$, $p_{LPS}=0.0443$, $df_{2DG}=15$, $p_{2DG}=0.7103$. (h) Quantification of TSPO expression following 24 h LPS or 2DG stimulation. One-way ANOVA with Dunnett's multiple comparisons test, $df_{LPS}=15$, $p_{LPS}=0.0477$, $df_{2DG}=15$, $p_{2DG}=0.9839$. (a–h) $n=6$, 60 mm dishes. kDa, kilodaltons; L, ladder. $^{*}p<0.05$, $^{****}p<0.0001$. Data are expressed as mean ± standard error of the mean.

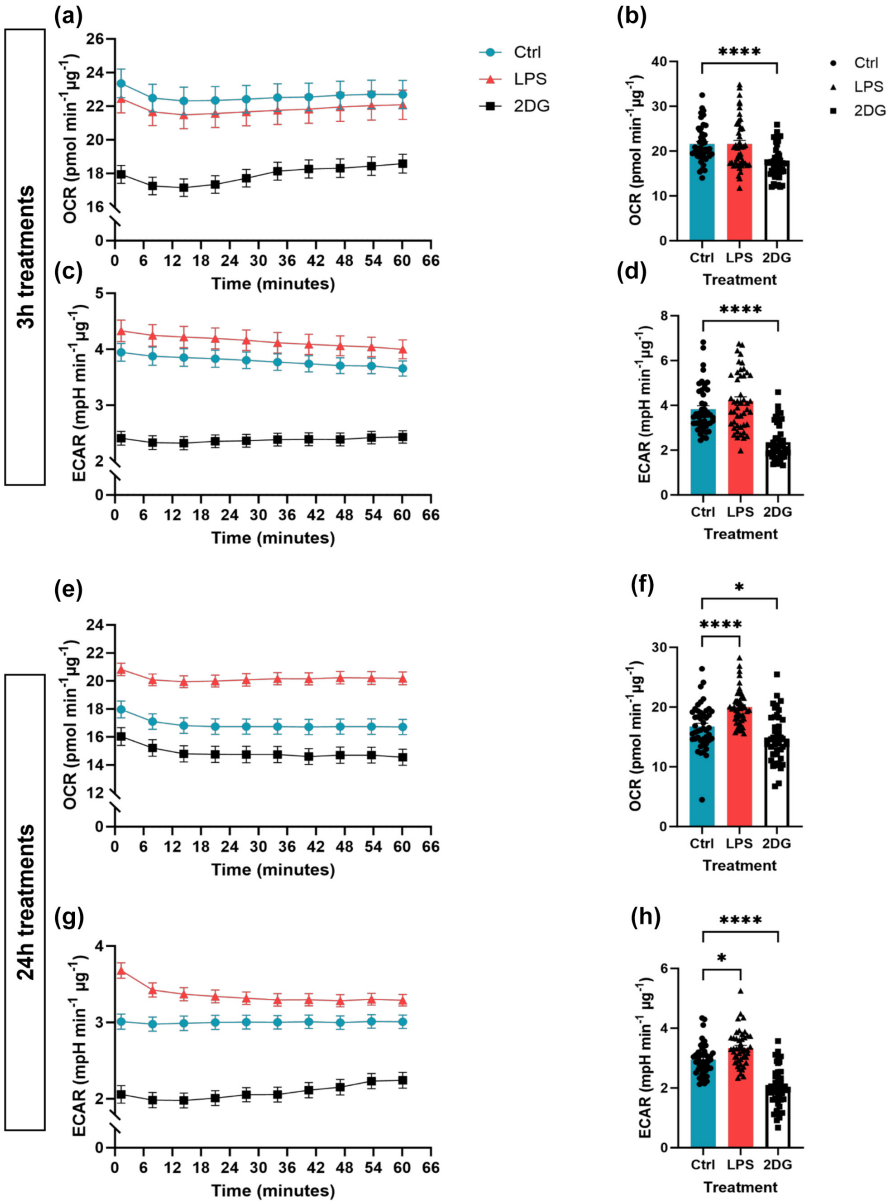


**FIGURE 8** 24 h LPS stimulation enhanced mitochondrial and non-mitochondrial respiration in C57BL/6J MPAs. (a) Oxygen consumption rate (OCR) of C57BL/6J MPAs treated with lipopolysaccharide (LPS; 100 ng/mL) or 2-deoxyglucose (2DG; 10 mM) for 3 h. (b) Quantification of (a), data are taken from time point 4. Ordinary one-way ANOVA with Dunnett's multiple comparisons test, $df_{LPS} = 133$, $p_{LPS} = 0.9996$, $df_{2DG} = 133$, $p_{2DG} < 0.0001$. (c) Extracellular acidification rate (ECAR) of C57BL/6J MPAs treated with LPS or 2DG for 3 h. (d) Quantification of (c), data are taken from time point 4. Kruskal–Wallis with Dunn's multiple comparisons test, $Z_{LPS} = 1.046$, $p_{LPS} = 0.5914$, $Z_{2DG} = 5.935$, $p_{2DG} < 0.0001$. (e) OCR of C57BL/6J MPAs treated with LPS or 2DG for 24 h. (f) Quantification of (e), data are taken from time point 4. Kruskal–Wallis with Dunn's multiple comparisons test, $Z_{LPS} = 4.097$, $p_{LPS} < 0.0001$, $Z_{2DG} = 2.258$, $p_{2DG} = 0.0479$. (g) ECAR of C57BL/6J MPAs treated with LPS or 2DG for 24 h. (h) Quantification of (g), data are taken from time point 4. Kruskal–Wallis with Dunn's multiple comparisons test, $Z_{LPS} = 2.695$, $p_{LPS} = 0.0141$, $Z_{2DG} = 5.256$, $p_{2DG} < 0.0001$. (a–h) $n = 46$–48 wells, data are pooled from across three independent plates. $^{*}p < 0.05$, $^{****}p < 0.0001$. Data are expressed as mean ± standard error of the mean.

inhibitor of glycolysis, 2DG, in Figures 7 and 8 as a positive control for a change in astrocyte metabolic state.

First, we confirmed that MPAs were undergoing an inflammatory response to LPS stimulation by assessing phosphorylation of nuclear factor kappa-B (p65) at Ser536, finding that this was significantly increased at both time points (NFκB; 3 h Figure 7a–c; $p < 0.0001$; 24 h Figure 7e–g; $p = 0.044$). While 3 h LPS stimulation did not significantly increase TSPO expression in MPAs (Figure 7a,d; $p = 0.99$), 24 h LPS stimulation induced a significant increase in TSPO expression (Figure 7e,h; $p = 0.048$). Neither 3 h nor 24 h 2DG stimulation significantly affected NFκB phosphorylation (Figure 7a,c [3 h], Figure 7e,g [24 h]; $p = 0.39$ [3 h], $p = 0.71$ [24 h]) or TSPO expression (Figure 7a,d [3 h], Figure 7e,h [24 h]; $p = 0.47$ [3 h], $p = 0.98$ [24 h]).

To confirm that the shift in TSPO expression was concomitant with a shift in the metabolic phenotype of MPAs, we next assessed LPS-induced changes in astrocyte metabolism. 3 h LPS stimulation did not significantly increase OCR (Figure 8a,b; $p = 0.99$) or ECAR (Figure 8c,d; $p = 0.59$) of MPAs, however, 24 h LPS stimulation increased MPA OCR (Figure 8e,f; $p < 0.0001$) and ECAR (Figure 8g,h; $p = 0.014$). 3 h 2DG stimulation significantly reduced MPA OCR (Figure 8a,b; $p < 0.0001$) and ECAR (Figure 8c,d; $p < 0.0001$). 24 h 2DG stimulation significantly reduced MPA OCR (Figure 8e,f; $p = 0.048$) and ECAR (Figure 8g,h; $p < 0.0001$). While 24 h 2DG stimulation significantly reduced cell viability, 24 h LPS stimulation did not (Figure S5). Though the MPA bioenergetics following 3 h LPS stimulation did not match those reported in our previous study (Robb et al., 2020), this can be attributed to the current study using different experimental conditions to the former study.

## 3.6 | TSPO deficiency altered the pattern of TNF secretion following LPS stimulation

Having confirmed that the shift in mouse primary astrocyte bioenergetics in response to 24 h LPS treatment was concomitant with

altered TSPO expression (Figures 7 and 8), we postulated that TSPO-deficient MPAs may show altered inflammatory and metabolic responses to LPS stimulation. We began by characterizing secretion of TNF from TSPO$^{-/-}$ MPAs following LPS stimulation (Figure 9). Following 3 h LPS stimulation, we observed a statistically significant effect of genotype (Figure 9a; $p_{genotype}<0.0001$, $F_{(1,16)}=141.2$) and LPS stimulation ($p_{LPS}=0.0007$, $F_{(1,16)}=17.41$) on TNF secretion, as well as a statistically significant interaction of these variables ($p_{interaction}=0.0007$, $F_{(1,16)}=17.41$). Likewise, following 24 h LPS stimulation, we observed a statistically significant effect of genotype (Figure 9b; $p_{genotype}=0.01$, $F_{(1,20)}=8.038$) and LPS stimulation ($p_{LPS}<0.0001$, $F_{(1,20)}=91.97$) on TNF secretion in addition to a statistically significant interaction of these variables ($p_{interaction}=0.01$, $F_{(1,20)}=8.038$). Post-hoc analyses confirmed that in response to 3 h LPS stimulation, TNF secretion from TSPO$^{-/-}$ MPAs was reduced by 52.0% compared to TSPO$^{+/+}$ controls (Figure 9a; $p=0.0001$). In contrast, after 24 h LPS stimulation, we found that TSPO$^{-/-}$ MPAs released 183.9% more TNF than TSPO$^{+/+}$ controls (Figure 9b, $p=0.0035$).

As a key regulator of the inflammatory response, altered NFκB phosphorylation in TSPO$^{-/-}$ MPAs may have contributed to this. However, we observed no statistically significant effect of genotype (Figure 10a–c; $p_{genotype}=0.3408$, $F_{(1,19)}=0.95$) on NFκB phosphorylation following 3 h LPS stimulation, but as anticipated we observed a significant effect of LPS stimulation on NFκB phosphorylation following 3 h stimulation ($p_{LPS}<0.0001$, $F_{(1,19)}=41.95$). We observed no statistically significant interaction between TSPO genotype and 3 h LPS stimulation ($p_{interaction}=0.18$, $F_{(1,19)}=1.911$). Likewise, following 24 h LPS stimulation, we observed no statistically significant effect of genotype (Figure 10d–f; $p_{genotype}=0.97$, $F_{(1,19)}=0.001168$). However, we observed a statistically significant effect of 24 h LPS stimulation on NFκB phosphorylation ($p_{LPS}<0.0001$, $F_{(1,19)}=25.52$). There was no statistically significant interaction between these variables ($p_{interaction}=0.57$, $F_{(1,19)}=0.3276$). Post-hoc assessment confirmed no significant difference in NFκB phosphorylation in TSPO$^{-/-}$ MPAs compared to TSPO$^{+/+}$ controls following either 3 h (Figure 10a–c; $p=0.48$) or 24 h LPS stimulation (Figure 10d–f; $p=0.99$).

## 3.7 | Mouse primary astrocyte TSPO deficiency did not impact the metabolic response following LPS stimulation

We hypothesized that the altered cytokine secretion profile observed in TSPO$^{-/-}$ MPAs might reflect a different metabolic response to LPS in these cells, related to their altered metabolic profile (Figures 1–5).

Following 3 h LPS stimulation, the statistically significant impact of genotype on MPA metabolic parameters seen in earlier experiments (Figure 1) was maintained (Figure 11a–d; OCR: $p_{genotype}<0.0001$, $F_{(1,66)}=18.45$; ECAR: $p_{genotype}=0.0019$, $F_{(1,64)}=10.51$). However, using a two-way ANOVA we observed no statistically significant effect of 3 h LPS stimulation on MPA bioenergetics (OCR $p_{LPS}=0.54$, $F_{(1,66)}=0.3802$; ECAR $p_{LPS}=0.72$, $F_{(1,20)}=0.1259$), and observed no statistically significant interaction between genotype and 3 h LPS stimulation (Figure 11a–d; OCR: $p_{interaction}=0.26$, $F_{(1,66)}=1.3002$; ECAR: $p_{interaction}=0.64$, $F_{(1,64)}=0.2173$). Post-hoc analysis revealed that, in line with our previous data from C57BL/6J MPAs (Figure 7), neither the OCR nor ECAR of TSPO$^{+/+}$ MPAs significantly changed in response to 3 h LPS stimulation (Figure 11a–d; $p=0.66$ [OCR], $p=0.99$ [ECAR]).

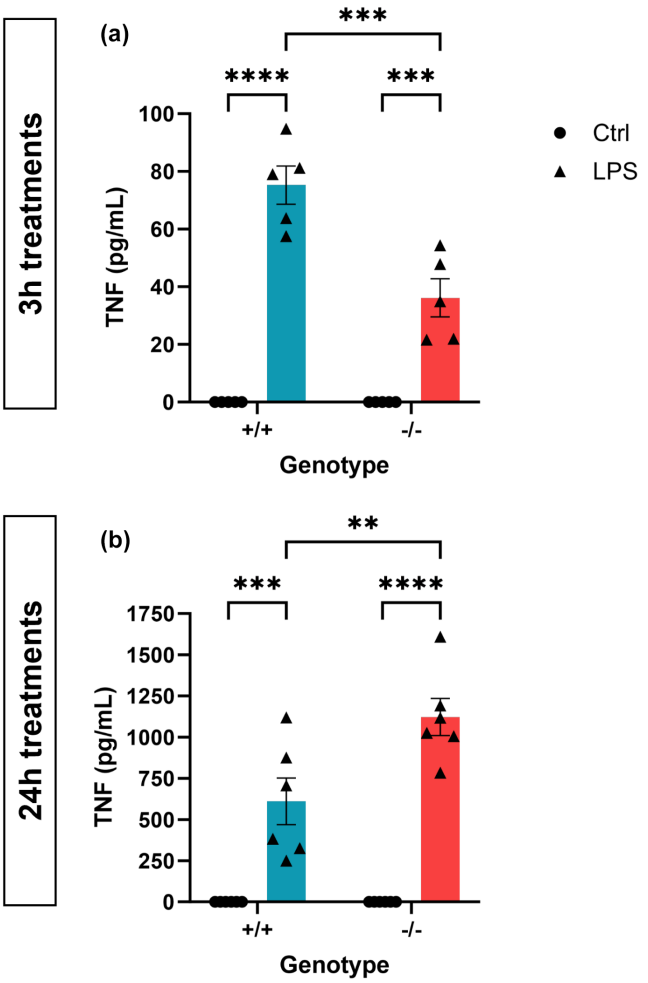


FIGURE 9 TSPO deficiency modulated cytokine release from MPAs. (a, b) Tumor necrosis factor (TNF) secretion from TSPO-deficient (TSPO$^{-/-}$) MPAs and wildtype (TSPO$^{+/+}$) controls following 3 h (a) or 24 h (b) lipopolysaccharide (LPS; 100 ng/mL) stimulation. (a) 2-way ANOVA with Šídák's multiple comparisons test, $p_{genotype}<0.0001$, $F_{(1,16)}=141.2$. $p_{LPS}=0.0007$, $F_{(1,16)}=17.41$. $p_{interaction}=0.0007$, $F_{(1,16)}=17.41$. Post-hoc analysis revealed that TNF secretion from TSPO$^{-/-}$ MPAs was significantly reduced compared to TSPO$^{+/+}$ controls in response to 3 h LPS stimulation ($p=0.0001$). (b) 2-way ANOVA with Šídák's multiple comparisons test, $p_{genotype}=0.0102$, $F_{(1,20)}=8.038$. $p_{LPS}<0.0001$, $F_{(1,20)}=91.97$. $p_{interaction}=0.0102$, $F_{(1,20)}=8.038$. Post-hoc analysis revealed that TNF secretion from TSPO−/− MPAs was significantly increased compared to TSPO+/+ controls in response to 24 h LPS stimulation ($p=0.0035$). (a) $n=5$, 60 mm dishes. (b) $n=6$, 60 mm dishes. $^{**}p<0.01$, $^{***}p<0.001$, $^{****}p<0.0001$. Data are expressed as mean ± standard error of the mean.

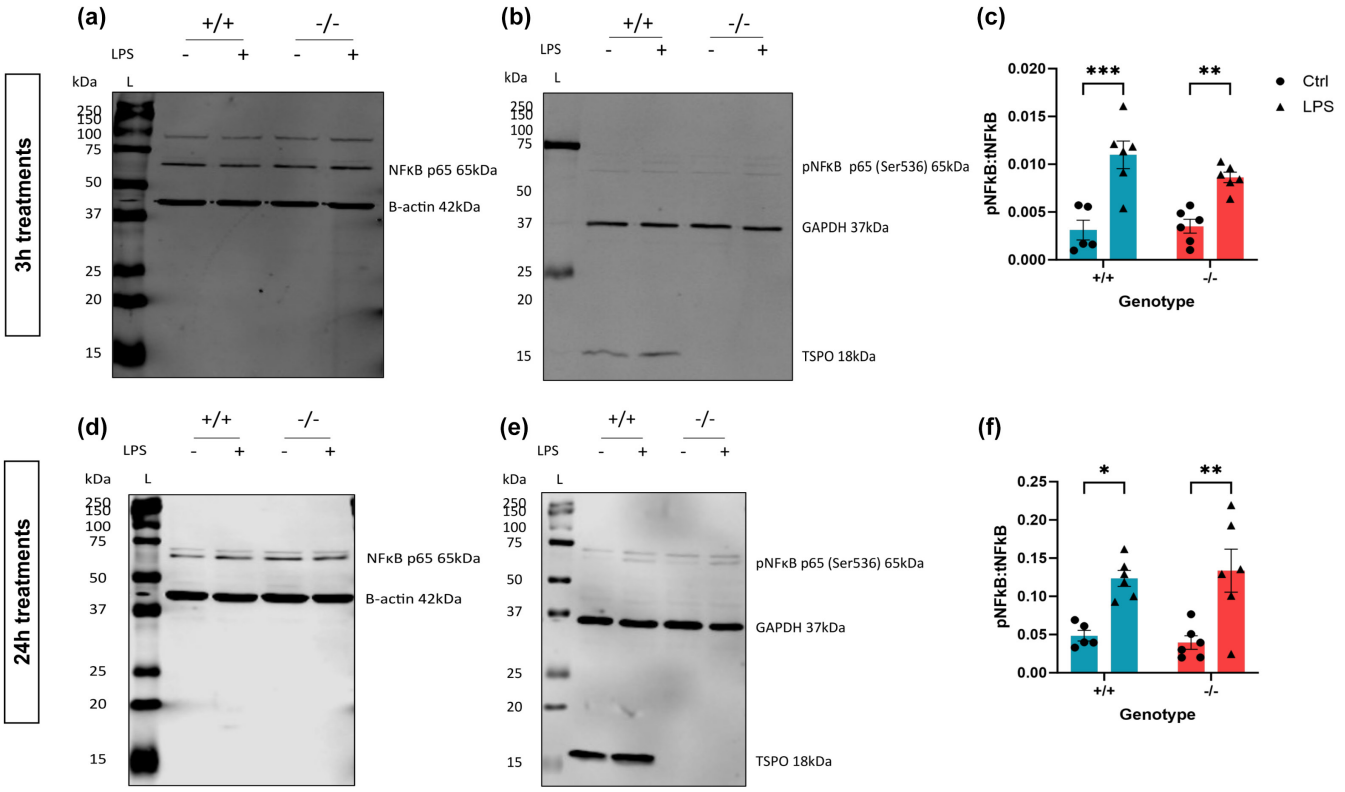


**FIGURE 10** Translocator protein 18 kDa (TSPO) deficiency did not modulate NFκB activation following lipopolysaccharide (LPS) stimulation. (a, b) Representative immunoblots of cell lysate from Figure 9a. (a) Representative immunoblot for total nuclear factor kappa B p65 (NFκB, tNFκB) and β-actin (B-actin) 3 h ± LPS (100 ng/mL) stimulation. (b) Representative immunoblot for phosphorylated NFκB p65 (Ser536; pNFκB), glyceraldehyde phosphate dehydrogenase (GAPDH), TSPO 3 h ± LPS stimulation. (c) Quantification of NFκB activation following 3 h ± LPS stimulation expressed as the ratio of pNFκB:NFκB. 2-way ANOVA with Šídák's multiple comparisons test, $p_{genotype} = 0.3408$, $F_{(1,19)} = 0.9547$. $p_{LPS} < 0.0001$, $F_{(1,19)} = 41.95$. $p_{interaction} = 0.1829$, $F_{(1,19)} = 1.911$. (d, e) Representative immunoblots of cell lysate from Figure 9B. (d) Representative immunoblot for tNFκB and β-actin 24 h ± LPS stimulation. (e) Representative immunoblot for pNFκB (Ser536), GAPDH, and TSPO 24 h ± LPS stimulation. (f) Quantification of NFκB activation following 24 h ± LPS stimulation expressed as the ratio of pNFκB:NFκB. 2-way ANOVA with Šídák's multiple comparisons test, $p_{genotype} = 0.9731$, $F_{(1,19)} = 0.001168$. $p_{LPS} < 0.0001$, $F_{(1,19)} = 25.52$. $p_{interaction} = 0.5738$, $F_{(1,19)} = 0.3276$. (a–f) n = 6, 60 mm dishes. kDa, kilodaltons; L, ladder. $^{*}p < 0.05$, $^{**}p < 0.01$, $^{***}p < 0.001$. Data are expressed as mean ± standard error of the mean.

Following our 24 h LPS stimulation paradigm overall there was no statistically significant impact of TSPO genotype on MPA OCR (Figure 11e–h; $p_{genotype} = 0.49$, $F_{(1,78)} = 0.4818$) or ECAR ($p_{genotype} = 0.54$, $F_{(1,78)} = 0.3704$). LPS stimulation significantly impacted both OCR ($p_{LPS} < 0.0001$, $F_{(1,78)} = 52.35$) and ECAR ($p_{LPS} < 0.0001$, $F_{(1,78)} = 28.89$), but there was not a statistically significant interaction between genotype and 24 h LPS stimulation (OCR: $p_{interaction} = 0.084$, $F_{(1,78)} = 3.055$; ECAR: $p_{interaction} = 0.41$, $F_{(1,78)} = 0.6742$). However, post-hoc analyses revealed that, in response to 24 h LPS stimulation, both OCR and ECAR increased in $TSPO^{+/+}$ (Figure 11f, 29.0% [OCR], $p = 0.003$; Figure 11h, 29.1% [ECAR], $p = 0.02$) and $TSPO^{-/-}$ MPAs (Figure 11f, 54.4% [OCR], $p < 0.0001$; Figure 11h, 40.1% [ECAR], $p < 0.0001$). Despite this, there was no statistically significant difference in the metabolic responses of $TSPO^{-/-}$ MPAs to 24 h LPS stimulation compared to $TSPO^{+/+}$ controls (Figure 11f,h; $p = 0.87$ [OCR], $p = 0.74$ [ECAR]).

We also assessed changes in expression of glucose transporter 1 (GLUT1), which we have previously shown to be modulated by 24 h but not 3 h LPS stimulation in MPAs (Robb et al., 2020). We observed neither a statistically significant impact of TSPO genotype (Figure 12a,b; $p_{genotype} = 0.87$, $F_{(1,19)} = 0.027$) nor of 3 h LPS stimulation on GLUT1 expression ($p_{LPS} = 0.63$, $F_{(1,19)} = 0.24$). We did not observe a statistically significant interaction between 3 h LPS stimulation and TSPO genotype on GLUT1 expression ($p_{interaction} = 0.17$, $F_{(1,19)} = 2.0$). Post-hoc analyses found no significant effect of genotype on GLUT1 expression at baseline or following 3 h LPS stimulation in these cells, which showed the same response as $TSPO^{+/+}$ controls (Figure 12a,b; $p = 0.96$).

In contrast to our expectations, following 24 h LPS stimulation, TSPO genotype had no statistically significant impact on GLUT1 expression (Figure 12e,f; $p_{genotype} = 0.52$, $F_{(1,20)} = 0.42$). In line with our previous study (Robb et al., 2020), 24 h LPS stimulation had a statistically significant impact on GLUT1 expression (Figure 12e,f; $p_{LPS} < 0.0001$, $F_{(1,20)} = 89.35$), but we observed no statistically significant interaction between TSPO genotype and LPS stimulation on GLUT1 expression ($p_{interaction} = 0.34$, $F_{(1,20)} = 0.91$). Using post-hoc analyses, we found that as with wildtype controls, GLUT1 expression was similarly reduced by 24 h LPS stimulation

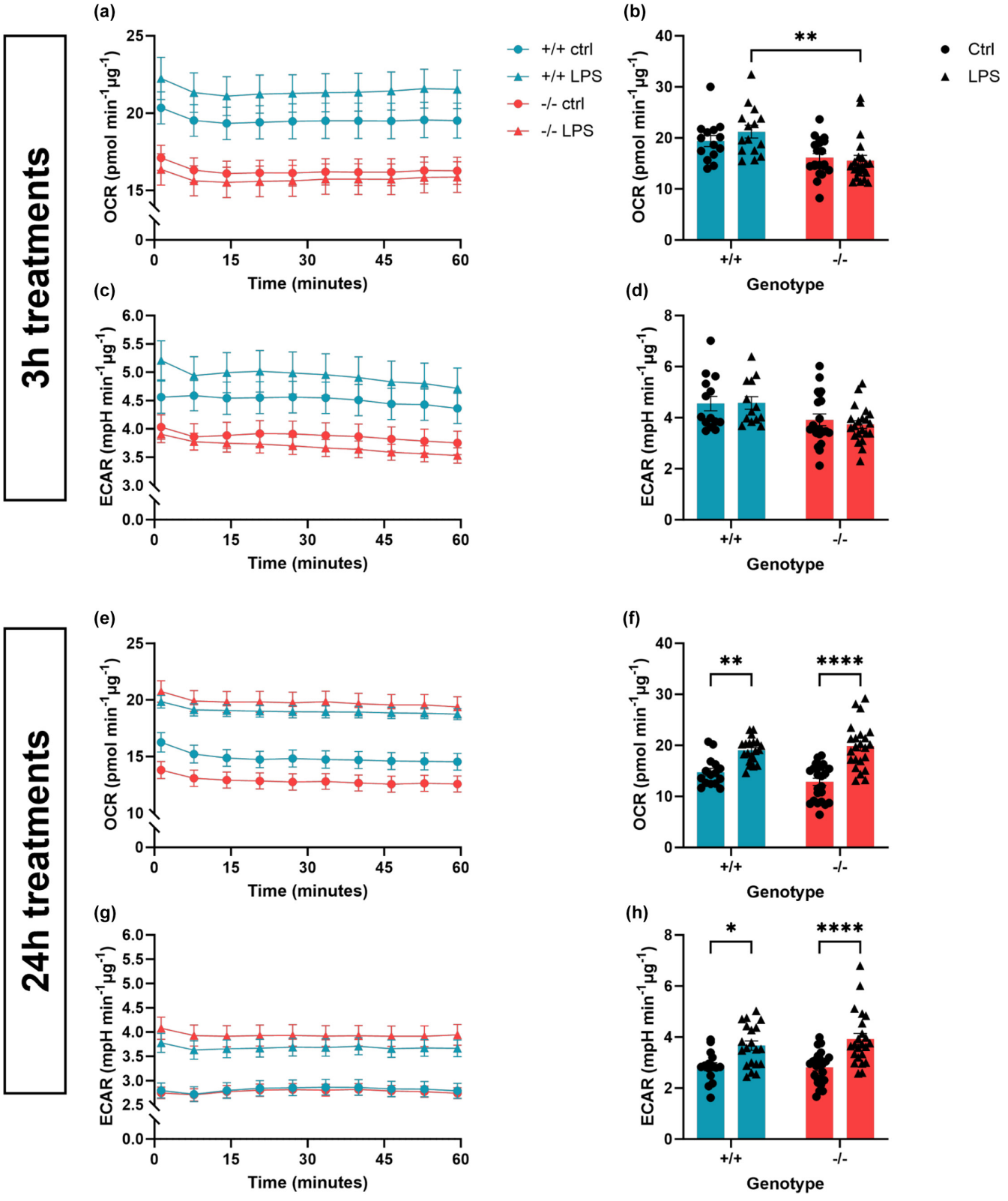


in MPAs (Figure 12e,f; $p < 0.0001$) regardless of TSPO genotype (Figure 12e,f; $p > 0.99$).

Previous work examining the role of TSPO in cellular metabolism has linked TSPO deficiency to increased expression of the *Cpt1a* gene in MA-10 Leydig cells (Tu et al., 2016), however, to the best of our knowledge, complementary changes to the expression of the CPT1a protein in astrocytes following genetic ablation of TSPO have not been evaluated. We observed no statistically significant effect of TSPO genotype (Figure 12c,d; $p_{genotype} = 0.70$, $F_{(1,20)} = 0.16$) or 3 h LPS stimulation ($p_{LPS} = 0.57$, $F_{(1,20)} = 0.33$) on CPT1a expression, and

**FIGURE 11** Translocator protein 18 kDa (TSPO) deficiency did not affect the metabolic response of MPAs to inflammatory stimulation. (a) Oxygen consumption rate (OCR) of TSPO-deficient ($TSPO^{-/-}$) MPAs and wildtype ($TSPO^{+/+}$) controls 3 h ± lipopolysaccharide (LPS; 100 ng/mL) stimulation. (b) Quantification of (a), data were taken from time point 4. 2-way ANOVA with Tukey's multiple comparisons test, $p_{genotype} < 0.0001$, $F_{(1,66)} = 18.45$. $p_{LPS} = 0.5396$, $F_{(1,66)} = 0.3802$. $p_{interaction} = 0.2579$, $F_{(1,66)} = 1.3002$. (c) Extracellular acidification rate (ECAR) of $TSPO^{-/-}$ MPAs and $TSPO^{+/+}$ controls 3 h ± LPS stimulation. (d) Quantification of (c), data were taken from timepoint 4. 2-way ANOVA with Tukey's multiple comparisons test, $p_{genotype} = 0.0019$, $F_{(1,64)} = 10.51$. $p_{LPS} = 0.7230$, $F_{(1,20)} = 0.1259$. $p_{interaction} = 0.6427$, $F_{(1,64)} = 0.2173$. (e) OCR of $TSPO^{-/-}$ MPAs and $TSPO^{+/+}$ controls 24 h ± LPS stimulation. (f) Quantification of (e), data were taken from timepoint 4. 2-way ANOVA with Tukey's multiple comparisons test, $p_{genotype} = 0.4897$, $F_{(1,78)} = 0.4818$. $p_{LPS} < 0.0001$, $F_{(1,78)} = 52.35$. $p_{interaction} = 0.0844$, $F_{(1,78)} = 3.055$. (g) ECAR of $TSPO^{-/-}$ MPAs and $TSPO^{+/+}$ controls 24 h ± LPS stimulation. (h) Quantification of (g), data were taken from timepoint 4. 2-way ANOVA with Tukey's multiple comparisons test, $p_{genotype} = 0.5445$, $F_{(1,78)} = 0.3704$. $p_{LPS} < 0.0001$, $F_{(1,78)} = 28.89$. $p_{interaction} = 0.4141$, $F_{(1,78)} = 0.6742$. (a–d) $n = 15$–21 wells per group, data are pooled from across two independent plates. (e–h) $n = 15$–24 wells per group, data are pooled from across two independent plates. $^{*}p < 0.05$, $^{**}p < 0.01$, $^{****}p < 0.0001$. Data are expressed as mean ± standard error of the mean.

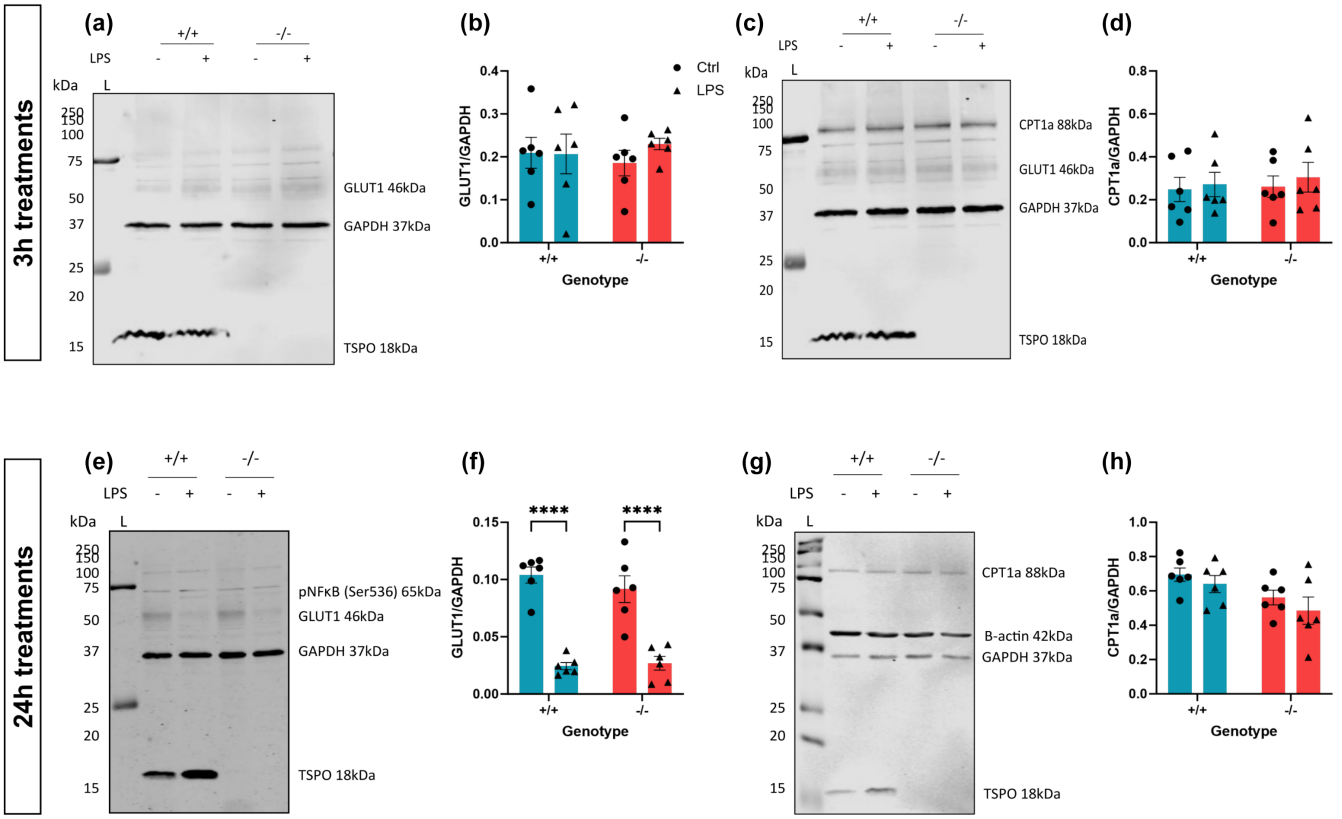


**FIGURE 12** Inflammation-induced changes to GLUT1 and CPT1a expression were not modulated by TSPO deficiency. (a) Representative immunoblot of cell lysate from Figure 9a for GLUT1 following 3 h LPS stimulation. (b) Quantification of (a). 2-way ANOVA with Šídák's multiple comparisons test, $p_{genotype} = 0.9904$, $F_{(1,20)} = 0.0001496$. $p_{LPS} = 0.5423$, $F_{(1,20)} = 0.3843$. $p_{interaction} = 0.4914$, $F_{(1,20)} = 0.4914$. (c) Representative immunoblot of cell lysate from Figure 9a for CPT1a following 3 h LPS stimulation. (d) Quantification of (c). 2-way ANOVA with Šídák's multiple comparisons test, $p_{genotype} = 0.6950$, $F_{(1,20)} = 0.1582$. $p_{LPS} = 0.5721$, $F_{(1,20)} = 0.3300$. $p_{interaction} = 0.8628$, $F_{(1,20)} = 0.03066$. (e) Representative immunoblot of cell lysate from Figure 9b for GLUT1 following 24 h LPS stimulation. (f) Quantification of (e). 2-way ANOVA with Šídák's multiple comparisons test, $p_{genotype} = 0.5249$, $F_{(1,20)} = 0.4188$. $p_{LPS} < 0.0001$, $F_{(1,20)} = 89.35$. $p_{interaction} = 0.3435$, $F_{(1,20)} = 0.9413$. (g) Representative immunoblot of cell lysate from Figure 9b for CPT1a following 24 h LPS stimulation. (h) Quantification of (g). 2-way ANOVA with Šídák's multiple comparisons test, $p_{genotype} = 0.0165$, $F_{(1,20)} = 6.848$. $p_{LPS} = 0.2485$, $F_{(1,20)} = 1.413$. $p_{interaction} = 0.8470$, $F_{(1,20)} = 0.03820$. (a–h) $n = 6$, 60 mm dishes. kDa, kilodaltons; L, ladder. $^{****}p < 0.0001$. Data are expressed as mean ± standard error of the mean.

observed no statistically significant interaction between these two variables ($p_{interaction} = 0.86$, $F_{(1,20)} = 0.0031$). In contrast, using our 24 h LPS stimulation model, we observed a statistically significant effect of genotype on CPT1a expression (Figure 12g,h; $p_{genotype} = 0.017$, $F_{(1,20)} = 6.8$). However, we observed no statistically significant effect of 24 h LPS stimulation on CPT1a expression ($p_{LPS} = 0.25$, $F_{(1,20)} = 1.4$), nor did we observe an interaction between TSPO genotype and 24 h LPS stimulation ($p_{interaction} = 0.85$, $F_{(1,20)} = 0.038$). Post-hoc analysis confirmed that CPT1a expression was unchanged by TSPO genotype at baseline or following 3 h (Figure 12e,f; $p = 0.99$ [$TSPO^{+/+}$], $p = 0.95$ [$TSPO^{-/-}$]) or 24 h LPS stimulation (Figure 12g,h; $p = 0.89$ [$TSPO^{+/+}$], $p = 0.76$ [$TSPO^{-/-}$]).

## 4 | DISCUSSION

TSPO, a protein linked to a variety of cellular processes including regulation of cellular metabolism and inflammatory responses, has previously been demonstrated to play a role in fatty acid metabolism in the periphery (Koganti & Selvaraj, 2020; Li et al., 2021; Tu et al., 2016). Two key facets remain unclear: firstly, whether this happens in all cell types, and secondly, by what underlying mechanisms TSPO may be involved with FAO. In this study, we provide data supporting the hypothesis that TSPO regulates cellular bioenergetics in MPAs and the U373 astrocytoma cell line. We showed that not only do TSPO$^{-/-}$ MPAs and U373 astrocytoma cells secrete less lactate than wildtype controls, but also that these cells are more reliant on FAO to meet their bioenergetic requirements. In support of our bioenergetics data, using co-immunoprecipitations we have for the first time experimentally demonstrated the existence of an interaction between TSPO and the rate-limiting enzyme in FAO, CPT1a, thus providing a possible mechanism through which TSPO may regulate FAO. Moreover, we showed here that in MPAs TSPO deficiency did not restrict the metabolic response of these cells to an inflammatory stimulus, nor did it alter their expression of key metabolic proteins in response to inflammation, but may alter the temporal profile of the MPA inflammatory response.

### 4.1 | TSPO as a regulator of astrocyte metabolism

In other glial and non-glial cells, TSPO deficiency has been linked to reduced oxidative phosphorylation and glycolysis (Da Pozzo et al., 2019; Fairley et al., 2023; Fu et al., 2020; Tu et al., 2016; Yao et al., 2020). In line with these studies, we found that TSPO deficiency in MPAs and U373 astrocytoma cells reduced basal mitochondrial metabolism and non-mitochondrial respiration. Furthermore, in agreement with a recent study in microglia (Yao et al., 2020), we found that TSPO deficiency enhances the metabolic response in MPAs following the injection of a supraphysiological glucose concentration during the glycolysis stress test. This may be interpreted as increased glycolytic rate in TSPO$^{-/-}$ MPAs. During a nutrient deficit simulated by exposing the cells to a glucose-free condition for 1 h, we found that TSPO-deficient MPAs and U373 astrocytoma cells lacked the metabolic adaptations observed in their TSPO-expressing control counterparts. Moreover, we found that the bioenergetic rates of TSPO$^{-/-}$ MPAs did not change significantly between glucose and glucose-free conditions, and TSPO$^{-/-}$ MPAs and U373 astrocytoma cells secreted significantly less L-lactate in the presence of glucose. This contrasts with a recent publication demonstrating that TSPO deficiency in microglia increases lactate production and glycolysis (Fairley et al., 2023), but nonetheless is supportive of our data indicating altered metabolic substrate utilization in TSPO$^{-/-}$ MPAs and U373 astrocytoma cells. Importantly, the difference between our findings in astrocytes and the findings of Fairley et al. (2023) may be due to fundamental differences in the metabolic machinery of astrocytes (which express relatively high amounts of CPT1a (Jernberg et al., 2017)) and microglia (which express less CPT1a than astrocytes (Bernier et al., 2020; Jernberg et al., 2017)) underlying the resulting metabolic profile. Crucially, our data show that the basal bioenergetic rates of TSPO$^{-/-}$ MPAs and U373 astrocytoma cells are reduced relative to TSPO$^{+/+}$ controls. This is reinforced by our finding that TSPO$^{-/-}$ MPAs and U373 astrocytoma cells secrete less L-lactate than their respective TSPO$^{+/+}$ controls (Figure 4e,f), implying that this may be caused either by reduced glucose metabolism, or more efficient funneling of glycolytic end products to oxidative phosphorylation.

As we did not directly quantify pyruvate production in these cells our L-lactate data alone cannot inform us whether TSPO$^{-/-}$ MPAs oxidize a greater amount of lactate than wildtype controls. Because mitochondrial pyruvate metabolism consumes oxygen, one may therefore anticipate that enhanced mitochondrial pyruvate metabolism would elicit a concomitant increase in OCR in TSPO$^{-/-}$ astrocytes. However, when exogenous glucose was unavailable as a substrate, we saw no significant increase in the OCR of TSPO$^{-/-}$ MPAs (Figure 4a–d). Thus, we argue that the decrease in L-lactate secreted by TSPO$^{-/-}$ MPAs relative to TSPO$^{+/+}$ controls indicates that TSPO$^{-/-}$ MPAs are likely less dependent on glucose to meet their bioenergetic requirements. This is further supported by our finding that removal of glucose from the extracellular media resulted in no change in lactate secretion, OCR or ECAR in TSPO$^{-/-}$ MPAs (Figure 4). More widely, this suggests that TSPO deficiency may enable enhanced metabolic flexibility in astrocytes, potentially facilitating metabolism of other fuel sources even when glucose is available as a metabolic substrate. Therefore, we speculated that TSPO$^{-/-}$ MPAs may have been better able to utilize alternative metabolic substrates.

### 4.2 | Regulation of FAO in astrocytes by TSPO

In the published literature, TSPO has been shown to regulate fatty acid oxidation (FAO) in Leydig cells (Tu et al., 2016) and hepatocytes (Li et al., 2021). We thus postulated that the differences in TSPO$^{-/-}$ MPA and U373 astrocytoma cell bioenergetics may be explained by FAO making a larger contribution to maintaining basal metabolic rates in these cells. Using the FAO stress test paradigm (Figure 5a), we found that TSPO$^{-/-}$ MPAs indeed utilized more fatty acids to maintain their basal bioenergetic needs: OCR was increased in TSPO$^{-/-}$ MPAs supplemented with palmitate compared to those supplemented with palmitate and treated with etomoxir, a potent inhibitor of CPT1a, implying that FAO formed a larger part of the metabolic base of TSPO$^{-/-}$ MPAs compared to wildtype MPAs (Figure 5b). This shows that TSPO plays a role in regulating FAO in astrocytes, key homeostatic cells of the CNS. In U373 astrocytoma cells, we observed no statistically significant difference in the contribution of FAO to maintaining basal mitochondrial respiration, however there was an increased contribution of FAO to maximal mitochondrial respiration in these cells. This may be due to the increased reliance on glycolysis observed in glioma (Stanke et al., 2021) which may be

facilitated by the widely-reported increases in TSPO expression in glioma (Ammer et al., 2020); however, when we compared basal TSPO expression in MPAs to U373 astrocytoma cells, we observed no statistically significant difference in TSPO expression in U373 astrocytoma cells (though TSPO expression trended toward an increase in U373 astrocytoma cells; Figure S4D,E).

While the role of TSPO in regulating FAO has been reported before in other cell types (Koganti & Selvaraj, 2020; Li et al., 2021; Tu et al., 2016), a mechanism through which it is driven has only been speculated upon with, to our knowledge, no direct experimental confirmation. TSPO is reported to have multiple interacting partners, including VDAC (Gatliff & Campanella, 2016; Hiser et al., 2021), another constituent of the outer mitochondrial membrane, and metabolic proteins such as hexokinase-2 (Asih et al., 2022; Fairley et al., 2023). CPT1a and VDAC have been demonstrated to form a complex (Hu et al., 2023; Lee et al., 2011), indirectly suggesting that TSPO may also form part of this complex. However, to the best of our knowledge this has not yet been experimentally confirmed. Thus, we first used transfections to induce overexpression of a tagged TSPO construct in the in the U373 astrocytoma cell line, and observed that the tagged TSPO construct interacts with VDAC and also CPT1a (Figure 6a). We were then able to recapitulate this finding in the U373 astrocytoma cells without transfections using endogenous TSPO (Figure 6b,c), demonstrating that this interaction was not solely a result of introducing a tagged construct into cells. Finally, we were able to immunoprecipitate TSPO from whole cell lysate using a CPT1a pulldown and vice versa (Figure 6f,g), demonstrating that this interaction is conserved in MPAs. Together, these findings are supportive of the wider literature focusing on cells of the periphery where it has been shown that TSPO deficiency increases FAO, and overexpression of TSPO reduces expression of *Cpt1a* (Tu et al., 2016). Hence, we propose that this interaction is a likely mechanism by which TSPO regulates FAO in astrocytes. Overall, our data interrogating the role of TSPO in regulating astrocyte metabolism suggests that TSPO deficiency promotes FAO and implies that, when present, TSPO may regulate FAO in these cells.

### 4.3 | Impact of TSPO deficiency on the mouse primary astrocyte metabolic response to inflammation

Studies in peripheral immune cells have demonstrated that during the resolutory phase of inflammatory responses FAO is increased at the expense of glycolysis (O'Neill et al., 2016), though this remains controversial (Batista-Gonzalez et al., 2020). Nonetheless, alongside the data we have presented here, the findings from these studies in peripheral immune cells correlate with our recent study that demonstrated chronic LPS stimulation enhances mitochondrial metabolism in astrocytes (Robb et al., 2020), which suggests a metabolic shift geared toward resolving inflammatory responses. Moreover, FAO in astrocytes has been linked to both beneficial and detrimental effects on the CNS depending on the context of the reactive response (Xiong et al., 2022). In our data, when mitochondrial stress responses were assessed during the FAO paradigm using the uncoupling agent FCCP we found that $TSPO^{-/-}$ MPAs used more FAO to fuel their response (Figure 5c). This led us to speculate that the bioenergetic response of $TSPO^{-/-}$ MPAs to inflammatory stimulation may be modulated by enhanced basal FAO associated with TSPO deficiency (Figure 5b; Tu et al., 2016); however, our experimental findings did not reflect this hypothesis. Indeed, we found that the bioenergetic phenotype of $TSPO^{-/-}$ MPAs in response to LPS stimulation was not significantly different from $TSPO^{+/+}$ controls (Figure 11), suggesting that TSPO deficiency does not modulate the bioenergetic response of MPA to this stimulus. As we did not directly interrogate changes to FAO following LPS stimulation, we cannot provide further comment on whether enhanced FAO in $TSPO^{-/-}$ MPAs modulates the bioenergetic response. Despite this we have presented data suggesting an altered temporal release profile of TNF from $TSPO^{-/-}$ MPAs (Figure 9), though we only examined one concentration of one inflammatory stimulus at two time points. Regardless, this suggests that $TSPO^{-/-}$ MPAs may be predisposed to a resolutory response to inflammatory stimulation, thus explaining the temporal modulation of TNF release. Though the mechanism underlying our finding remains unclear, interrogating $Ca^{2+}$ dynamics in $TSPO^{-/-}$ astrocytes may be an interesting future area for study as TSPO has been linked to calcium signaling in mouse embryonic fibroblasts (Gatliff et al., 2017), neurons (Gatliff et al., 2017), and tanycytes (Kim et al., 2020), which may hint at a potential underlying mechanism distinct from a shift in the metabolic phenotype in astrocytes. $Ca^{2+}$ dynamics are an important signaling mechanism linked to various processes in astrocytes. Importantly, TNF secretion is dependent on the activity of a disintegrin and metalloprotease 17 (ADAM17) (Grötzinger et al., 2017; Moatti & Cohen, 2021), and the activity of ADAM17 is linked in part to the successful formation of the Nod-like receptor family pyrin domain containing 3 (NLRP3) inflammasome (Zheng et al., 2020). TSPO has been linked to the regulation of NLRP3 inflammasome formation in microglia (Guilarte et al., 2016; Loth et al., 2020) and the existence of this macrostructure has been evidenced in astrocytes (Dong et al., 2023; Lu et al., 2014). Moreover, mitochondrial $Ca^{2+}$ efflux has been implicated in this process (Gurung et al., 2015), suggesting that this may be a mechanism through which TSPO indirectly influences the secretion of proinflammatory cytokines. Future studies could further interrogate the mechanism by which TSPO regulates the reactive phenotype of astrocytes, perhaps via transcriptomic arrays, which we did not examine in this study so cannot provide comment on. This could be paired with a metabolomics array to better elucidate any differences in substrate utilization following 'acute' and 'chronic' proinflammatory stimulation of $TSPO^{-/-}$ astrocytes.

In vivo, under 'basal' (i.e., non-pathological) conditions, much CNS TSPO expression is accounted for by astrocytes (Betlazar et al., 2018), endothelial cells (Betlazar et al., 2018), and pericytes (Betlazar et al., 2018), with smaller contributions being attributed to microglia (Betlazar et al., 2018; Notter et al., 2021) and neurons (Betlazar et al., 2018; Notter et al., 2021). Interestingly,

expression of TSPO in neurons positively correlates with neuronal activity and oxidative phosphorylation (Guilarte et al., 2022; Notter et al., 2021), supporting a link between TSPO and regulation of cellular metabolism under 'basal' conditions in these cells. Furthermore, reactive astrocytes in vivo show increased TSPO expression (Lavisse et al., 2012) in a variety of pathophysiological contexts (Nutma et al., 2021; Tournier et al., 2020; Victorio et al., 2023; Winkeler et al., 2012), and we have previously demonstrated that astrocyte reactivity correlates with altered metabolism in these cells in vitro (Robb et al., 2020). Moreover, recent *in vitro* work using C6 astrocytoma cells has demonstrated that overexpression of TSPO increases ROS production and mitochondrial density while reducing glucose consumption, without altering mitochondrial membrane potential (Tournier et al., 2023). This is suggestive of a shift in cellular metabolism not dissimilar to the data presented in our current study, and perhaps indicates a change to TSPO stoichiometry in conditions where it is overexpressed, potentially to alter the bioenergetic state of astrocytes or fuel metabolic responses to prolonged (24 h [present study] or overnight (Tournier et al., 2023)) proinflammatory stimulation. In support of this, recent evidence from a murine model of Zika virus infection (Victorio et al., 2023) suggests that TSPO expression may correlate with the extent of glial reactivity or pathological severity (i.e., potential contribution to cellular hypermetabolism) with increased glial TSPO being observed within a relatively short timeframe. In 2020, Tournier et al. (2020) demonstrated that TSPO expression in astrocytes precedes increases of TSPO expression in microglia in a murine model of Alzheimer's disease. This is potentially important as the early stages of Alzheimer's disease correlate with a metabolic shift in the brain (Ardanaz et al., 2022). Given their widely acknowledged role in maintaining CNS homeostasis, increased TSPO expression in astrocytes during the early stages of this pathology may reflect a metabolic shift in these cells (Chen et al., 2017, Chen et al., 2023) that may help to support the development of a phenotype geared toward resolution of inflammation. This may be concomitant with a shift in the TSPO interactome or its stoichiometry in these reactive astrocytes, however this speculative hypothesis remains to be tested and could be addressed in future investigations.

Our data demonstrating a role for TSPO in regulating astrocyte metabolism and potentially impacting the release of TNF from MPAs may have implications when considering TSPO as a therapeutic target. Astrocytes are commonly thought to shuttle lactate to neurons for downstream metabolism (Mason, 2017). Here, we have reported that TSPO$^{-/-}$ MPAs and U373 astrocytoma cells secrete less lactate (Figure 4), implying that in the context of prolonged pharmacological TSPO-inhibition astrocytes may be less able to provide trophic support, in the form of lactate, to neurons as has been proposed elsewhere (Weightman Potter et al., 2019). Given recent evidence for the role of astrocytes in regulating memory formation (Zhou et al., 2021) and other behaviors (Jackson et al., 2020; MacDonald et al., 2020; Ortinski et al., 2022; Yang et al., 2015), and the crucial role of astrocyte CPT1a in cognition (Morant-Ferrando et al., 2023), prolonged inhibition of astrocyte TSPO may yield detrimental effects on cognitive and other neural functions which may need to be further investigated. In addition, astrocytes are highly plastic cells intrinsically involved with the maintenance of the brain microenvironment (Hart & Karimi-Abdolrezaee, 2021; Verkhratsky & Nedergaard, 2018). Perturbations to the ability of astrocytes to respond to noxious stimuli, including by modulating their metabolism—such as chronic neuroinflammation (Liddelow et al., 2020; Verkhratsky & Nedergaard, 2018)—may in turn impair the ability of these cells to resolve inflammation and restore homeostasis. While this impaired metabolic response to LPS-induced inflammation was not observed in our studies, we only looked at one inflammatory stimulus at one concentration, so additional comprehensive studies are required. While TSPO may serve as an attractive therapeutic target due to the proposed anti-inflammatory effects of its ligands (Azrad et al., 2019; Bader et al., 2019; Li et al., 2017; Monga et al., 2019, 2020; Zhou et al., 2020), if TSPO indeed functions as a regulator of metabolic flexibility in astrocytes, continuous pharmacological inhibition of TSPO function in these cells may blunt their ability to respond to inflammatory and other stimuli when chronically administered. However, a better understanding of the physiology and pharmacology of this protein is required prior to widespread clinical utilization.

## 5 | CONCLUSION

We have shown that TSPO deficiency reduced the basal metabolic rates of MPAs and U373 astrocytoma cells, reduced L-lactate secretion, and enabled MPAs to maintain their metabolic rates in the absence of glucose. Together these data suggest that TSPO deficient MPAs are less reliant on glucose to meet their energetic needs. Crucially, we have shown that the rate of FAO is increased in TSPO$^{-/-}$ MPAs and U373 astrocytoma cells and that, when present, TSPO forms a complex with CPT1a, providing a potentially mechanistic basis for how TSPO contributes to the regulation of FAO. This suggests that TSPO may ordinarily inhibit CPT1a function to conserve intracellular fat stores. Taken together, these data show that TSPO may act as a regulator of metabolic flexibility in astrocytes. Finally, we have shown that despite increases in basal FAO, the metabolic response to LPS stimulation is not impeded in TSPO$^{-/-}$ MPAs, though the release profile of the pro-inflammatory cytokine TNF is altered. Recapitulation of our results via pharmacological inhibition of TSPO will be important to decipher the therapeutic potential of this protein.

### AUTHOR CONTRIBUTIONS

**Wyn Firth:** Conceptualization; investigation; writing – original draft; methodology; writing – review and editing; formal analysis; data curation; funding acquisition. **Josephine L. Robb:** Conceptualization; investigation; writing – original draft; methodology; writing – review and editing; formal analysis; data curation. **Daisy Stewart:**

Investigation; writing – review and editing; data curation. **Katherine R. Pye:** Investigation; writing – review and editing. **Rosemary Bamford:** Supervision; writing – review and editing. **Asami Oguro-Ando:** Supervision; writing – review and editing. **Craig Beall:** Conceptualization; funding acquisition; supervision; writing – review and editing. **Kate L. J. Ellacott:** Conceptualization; data curation; funding acquisition; writing – original draft; writing – review and editing; supervision.

## ACKNOWLEDGEMENTS

This work was supported by grants from the British Society for Neuroendocrinology (WF) and Research England—Expanding Excellence in Diabetes award, and internal funding from the University of Exeter Medical School (which supported JLR). The TSPO-deficient mice were generated from material provided by the European Mouse Mutant Cell Repository through funding from the Medical Research Council, Grant/Award Number: MR/R014345/1 (to KLJE and CB). The authors extend their thanks to the Exeter BRF staff for facilitating and providing assistance with our animal work, and to Dr Ana Miguel Cruz, Dr Katie Partridge, Dr Paul Weightman Potter, Dr Jiping Zhang, and Asmaa Al-khalidi for their thoughts and insights.

All experiments were conducted in compliance with the ARRIVE guidelines.

## PEER REVIEW

The peer review history for this article is available at https://www.webofscience.com/api/gateway/wos/peer-review/10.1111/jnc.16089.

## DATA AVAILABILITY STATEMENT

The datasets used and analyzed during this study are available from the corresponding author upon receipt of reasonable request. A preprint of this article was posted on BioRxiv on 02-Oct-2023 (https://www.biorxiv.org/content/10.1101/2023.09.29.560159v1).

## ORCID

*Wyn Firth* https://orcid.org/0000-0001-6531-2580
*Josephine L. Robb* https://orcid.org/0000-0002-6955-7355
*Daisy Stewart* https://orcid.org/0009-0000-4155-1747
*Katherine R. Pye* https://orcid.org/0000-0002-0691-6007
*Rosemary Bamford* https://orcid.org/0000-0002-2107-4637
*Asami Oguro-Ando* https://orcid.org/0000-0003-4029-3250
*Craig Beall* https://orcid.org/0000-0002-4263-0866
*Kate L. J. Ellacott* https://orcid.org/0000-0001-5261-7465

## REFERENCES

Abbott, N. J., Rönnbäck, L., & Hansson, E. (2006). Astrocyte-endothelial interactions at the blood-brain barrier. *Nature Reviews. Neuroscience*, *7*(1), 41–53. https://doi.org/10.1038/nrn1824

Ammer, L. M., Vollmann-Zwerenz, A., Ruf, V., Wetzel, C. H., Riemenschneider, M. J., Albert, N. L., Beckhove, P., & Hau, P. (2020). The role of translocator protein TSPO in hallmarks of glioblastoma. *Cancers (Basel)*,*12*(10), 1–26. https://doi.org/10.3390/cancers12102973

Ardanaz, C. G., Ramírez, M. J., & Solas, M. (2022). Brain metabolic alterations in Alzheimer's disease. *International Journal of Molecular Sciences*, *23*(7), 3785. https://doi.org/10.3390/ijms23073785

Asih, P. R., Poljak, A., Kassiou, M., Ke, Y. D., & Ittner, L. M. (2022). Differential mitochondrial protein interaction profile between human translocator protein and its A147T polymorphism variant. *PLoS ONE*, *17*, e0254296. https://doi.org/10.1101/2021.07.23.453531

Azrad, M., Zeineh, N., Weizman, A., Veenman, L., & Gavish, M. (2019). The TSPO ligands 2-CL-MGV-1, MGV-1, and PK11195 differentially suppress the inflammatory response of BV-2 microglial cell to LPS. *International Journal of Molecular Sciences*, *20*(3), 1–14. https://doi.org/10.3390/ijms20030594

Bader, S., Wolf, L., Milenkovic, V. M., Gruber, M., Nothdurfter, C., Rupprecht, R., & Wetzel, C. H. (2019). Differential effects of TSPO ligands on mitochondrial function in mouse microglia cells. *Psychoneuroendocrinology*, *106*, 65–76. https://doi.org/10.1016/j.psyneuen.2019.03.029

Batista-Gonzalez, A., Vidal, R., Criollo, A., & Carreño, L. J. (2020). New insights on the role of lipid metabolism in the metabolic reprogramming of macrophages. *Frontiers in Immunology*, *10*(January), 1–7. https://doi.org/10.3389/fimmu.2019.02993

Benchling [Biology Software]. [Internet]. www.benchling.com

Bernier, L. P., York, E. M., Kamyabi, A., Choi, H. B., Weilinger, N. L., & MacVicar, B. A. (2020). Microglial metabolic flexibility supports immune surveillance of the brain parenchyma. *Nature Communications*, *11*(1), 1559. https://doi.org/10.1038/s41467-020-15267-z

Betlazar, C., Harrison-Brown, M., Middleton, R. J., Banati, R., & Liu, G. J. (2018). Cellular sources and regional variations in the expression of the neuroinflammatory marker translocator protein (TSPO) in the normal brain. *International Journal of Molecular Sciences*, *19*(9), 2707. https://doi.org/10.3390/ijms19092707

Betlazar, C., Middleton, R. J., Banati, R., & Liu, G. J. (2020). The translocator protein (TSPO) in mitochondrial bioenergetics and immune processes. *Cell*, *9*(2), 1–18. https://doi.org/10.3390/cells9020512

Bonsack, F., & Sukumari-Ramesh, S. (2018). TSPO: An evolutionarily conserved protein with elusive functions. *International Journal of Molecular Sciences*, *19*(6), 1694. https://doi.org/10.3390/ijms19061694

Cabezas, R., Ávila, M., Gonzalez, J., El-Bachá, R. S., Báez, E., García-Segura, L. M., Coronel, J. C. J., Capani, F., Cardona-Gomez, G. P., & Barreto, G. E. (2014). Astrocytic modulation of blood brain barrier: Perspectives on Parkinson's disease. *Frontiers in Cellular Neuroscience*, *8*(August), 1–11. https://doi.org/10.3389/fncel.2014.00211

Chen, W., Huang, Q., Lazdon, E., Gomes, A., Wong, M., Stephens, E., Royal, T. G., Frenkel, D., Cai, W., & Kahn, C. R. (2017). Loss of insulin signaling in astrocytes exacerbates Alzheimer-like phenotypes in a 5xFAD mouse model. *Proceedings of the National Academy of Sciences*, *120*, 2017. https://doi.org/10.1073/pnas.2220684120

Chen, Z., Yuan, Z., Yang, S., Zhu, Y., Xue, M., Zhang, J., & Leng, L. (2023). Brain energy metabolism: Astrocytes in neurodegenerative diseases. *CNS Neuroscience & Therapeutics*, *29*(1), 24–36. https://doi.org/10.1111/cns.13982

Da Pozzo, E., Tremolanti, C., Costa, B., Giacomelli, C., Milenkovic, V. M., Bader, S., Wetzel, C. H., Rupprecht, R., Taliani, S., Da Settimo, F., & Martini, C. (2019). Microglial pro-inflammatory and anti-inflammatory phenotypes are modulated by translocator protein activation. *International Journal of Molecular Sciences*, *20*(18), 1–21. https://doi.org/10.3390/ijms20184467

Dimitrova-Shumkovska, J., Krstanoski, L., & Veenman, L. (2020). Diagnostic and therapeutic potential of TSPO studies regarding neurodegenerative diseases, psychiatric disorders, alcohol use

disorders, traumatic brain injury, and stroke: An update. *Cell*, *9*(4), 870. https://doi.org/10.3390/cells9040870

Divakaruni, A. S., Hsieh, W. Y., Minarrieta, L., Duong, T. N., Kim, K. K. O., Desousa, B. R., Andreyev, A. Y., Bowman, C. E., Caradonna, K., Dranka, B. P., Ferrick, D. A., Liesa, M., Stiles, L., Rogers, G. W., Braas, D., Ciaraldi, T. P., Wolfgang, M. J., Sparwasser, T., Berod, L., … Murphy, A. N. (2018). Etomoxir inhibits macrophage polarization by disrupting CoA homeostasis. *Cell Metabolism*, *28*(3), 490–503.e7. https://doi.org/10.1016/j.cmet.2018.06.001

Dong, A. Q., Yang, Y. p., Jiang, S. m., Yao, X. y., Qi, D., Mao, C. j., Cheng, X. Y., Wang, F., Hu, L. F., & Liu, C. F. (2023). Pramipexole inhibits astrocytic NLRP3 inflammasome activation via Drd3-dependent autophagy in a mouse model of Parkinson's disease. *Acta Pharmacologica Sinica*, *44*(1), 32–43. https://doi.org/10.1038/s41401-022-00951-1

Downer, O. M., Marcus, R. E. G., Zürcher, N. R., & Hooker, J. M. (2020). Tracing the history of the human translocator protein to recent neurodegenerative and psychiatric imaging. *ACS Chemical Neuroscience*, *11*(15), 2192–2200. https://doi.org/10.1021/acschemneuro.0c00362

Escartin, C., Galea, E., Lakatos, A., O'Callaghan, J. P., Petzold, G. C., Serrano-Pozo, A., Steinhäuser, C., Volterra, A., Carmignoto, G., Agarwal, A., Allen, N. J., Araque, A., Barbeito, L., Barzilai, A., Bergles, D. E., Bonvento, G., Butt, A. M., Chen, W. T., Cohen-Salmon, M., … Verkhratsky, A. (2021). Reactive astrocyte nomenclature, definitions, and future directions. *Nature Neuroscience*, *24*, 312–325. https://doi.org/10.1038/s41593-020-00783-4

Fairley, L. H., Lai, K. O., Wong, J. H., Chong, W. J., Vincent, A. S., D'Agostino, G., Wu, X., Naik, R. R., Jayaraman, A., Langley, S. R., Ruedl, C., & Barron, A. M. (2023). Mitochondrial control of microglial phagocytosis by the translocator protein and hexokinase 2 in Alzheimer's disease. *Proceedings of the National Academy of Sciences of the United States of America*, *120*, 12. https://doi.org/10.1073/pnas.2209177120

Fairley, L. H., Sahara, N., Aoki, I., Ji, B., Suhara, T., Higuchi, M., & Barron, A. M. (2021). Neuroprotective effect of mitochondrial translocator protein ligand in a mouse model of tauopathy. *Journal of Neuroinflammation*, *18*(1), 1–13. https://doi.org/10.1186/s12974-021-02122-1

Fairley, L. H., Wong, J. H., & Barron, A. M. (2021). Mitochondrial regulation of microglial immunometabolism in Alzheimer's disease. *Frontiers in Immunology*, *12*(February), 1–10. https://doi.org/10.3389/fimmu.2021.624538

Fan, J., Lindemann, P., & Papadopoulos, V. (2012). Structural and functional evolution of the translocator protein (18 kDa). *Current Molecular Medicine*, *12*, 369–386. https://doi.org/10.2174/156652401120704036 9

Fu, Y., Wang, D., Wang, H., Cai, M., Li, C., Zhang, X., Chen, H., Hu, Y., Zhang, X., Ying, M., He, W., & Zhang, J. (2020). TSPO deficiency induces mitochondrial dysfunction, leading to hypoxia, angiogenesis, and a growth-promoting metabolic shift toward glycolysis in glioblastoma. *Neuro-Oncology*, *22*(2), 240–252. https://doi.org/10.1093/neuonc/noz183

Gatliff, J., & Campanella, M. (2016). TSPO: Kaleidoscopic 18-kDa amid biochemical pharmacology, control and targeting of mitochondria. *The Biochemical Journal*, *473*(2), 107–121. https://doi.org/10.1042/BJ20150899

Gatliff, J., East, D., Crosby, J., Abeti, R., Harvey, R., Craigen, W., Parker, P., & Campanella, M. (2014). TSPO interacts with VDAC1 and triggers a ROS-mediated inhibition of mitochondrial quality control. *Autophagy*, *10*(12), 2279–2296. https://doi.org/10.4161/15548627.2014.991665

Gatliff, J., East, D. A., Singh, A., Alvarez, M. S., Frison, M., Matic, I., Ferraina, C., Sampson, N., Turkheimer, F., & Campanella, M. (2017). A role for TSPO in mitochondrial Ca2+ homeostasis and redox stress signaling. *Cell Death & Disease*, *8*(6), 1–15. https://doi.org/10.1038/cddis.2017.186

González-García, I., Gruber, T., & García-Cáceres, C. (2021). Insulin action on astrocytes: From energy homeostasis to behaviour. *Journal of Neuroendocrinology*, *33*(4), 1–11. https://doi.org/10.1111/jne.12953

Grötzinger, J., Lorenzen, I., & Düsterhöft, S. (2017). Molecular insights into the multilayered regulation of ADAM17: The role of the extracellular region. *Biochimica et Biophysica Acta: Molecular Cell Research*, *1864*(11), 2088–2095. https://doi.org/10.1016/j.bbamcr.2017.05.024

Guilarte, T. R., Loth, M. K., & Guariglia, S. R. (2016). TSPO finds NOX2 in microglia for redox homeostasis. *Trends in Pharmacological Sciences*, *37*(5), 334–343. https://doi.org/10.1016/j.tips.2016.02.008

Guilarte, T. R., Rodichkin, A. N., McGlothan, J. L., Acanda De La Rocha, A. M., & Azzam, D. J. (2022). Imaging neuroinflammation with TSPO: A new perspective on the cellular sources and subcellular localization. *Pharmacology & Therapeutics*, *234*, 234. https://doi.org/10.1016/j.pharmthera.2021.108048

Gurung, P., Lukens, J. R., & Kanneganti, T. D. (2015). Mitochondria: Diversity in the regulation of the NLRP3 inflammasome. *Trends in Molecular Medicine*, *21*(3), 193–201. https://doi.org/10.1016/j.molmed.2014.11.008

Hart, C. G., & Karimi-Abdolrezaee, S. (2021). Recent insights on astrocyte mechanisms in CNS homeostasis, pathology, and repair. *Journal of Neuroscience Research*, *99*(10), 2427–2462. https://doi.org/10.1002/jnr.24922

Hernstadt, H., Wang, S., Lim, G., & Mao, J. (2009). Spinal translocator protein (TSPO) modulates pain behavior in rats with CFA-induced monoarthritis. *Brain Research*, *1286*, 42–52. https://doi.org/10.1016/j.brainres.2009.06.043

Hiser, C., Montgomery, B. L., & Ferguson-Miller, S. (2021). TSPO protein binding partners in bacteria, animals, and plants. *Journal of Bioenergetics and Biomembranes*, *53*(4), 463–487. https://doi.org/10.1007/s10863-021-09905-4

Houten, S. M., Violante, S., Ventura, F. V., & Wanders, R. J. A. (2016). The biochemistry and physiology of mitochondrial fatty acid $\beta$-oxidation and its genetic disorders. *Annual Review of Physiology*, *78*, 23–44. https://doi.org/10.1146/annurev-physiol-021115-105045

Hu, A., Wang, H., Xu, Q., Pan, Y., Jiang, Z., Li, S., Qu, Y., Hu, Y., Wu, H., & Wang, X. (2023). A novel CPT1A covalent inhibitor modulates fatty acid oxidation and CPT1A-VDAC1 axis with therapeutic potential for colorectal cancer. *Redox Biology*, *68*(September), 102959. https://doi.org/10.1016/j.redox.2023.102959

Jackson, F. R., You, S., & Crowe, L. B. (2020). Regulation of rhythmic behaviors by astrocytes. *Wiley Interdisciplinary Reviews: Developmental Biology*, *9*(4), 1–8. https://doi.org/10.1002/wdev.372

Jernberg, J. N., Bowman, C. E., Wolfgang, M. J., & Scafidi, S. (2017). Developmental regulation and localization of carnitine palmitoyltransferases (CPTs) in rat brain. *Journal of Neurochemistry*, *142*(3), 407–419. https://doi.org/10.1111/jnc.14072

Killen, M. J., Giorgi-Coll, S., Helmy, A., Hutchinson, P. J. A., & Carpenter, K. L. H. (2019). Metabolism and inflammation: Implications for traumatic brain injury therapeutics. *Expert Review of Neurotherapeutics*, *19*(3), 227–242. https://doi.org/10.1080/14737175.2019.1582332

Kim, S., Kim, N., Park, S., Jeon, Y., Lee, J., Yoo, S. J., Lee, J. W., Moon, C., Yu, S. W., & Kim, E. K. (2020). Tanycytic TSPO inhibition induces lipophagy to regulate lipid metabolism and improve energy balance. *Autophagy*, *16*(7), 1200–1220. https://doi.org/10.1080/15548627.2019.1659616

Koganti, P. P., & Selvaraj, V. (2020). Lack of adrenal TSPO/PBR expression in hamsters reinforces correlation to triglyceride metabolism. *The Journal of Endocrinology*, *247*(1), 1–10. https://doi.org/10.1530/JOE-20-0189

Kriegstein, A., & Alvarez-Buylla, A. (2009). The glial nature of embryonic and adult neural stem cells. *Annual Review of Neuroscience*, *32*, 149–184. https://doi.org/10.1146/annurev.neuro.051508.135600

Kuhlmann, A. C., & Guilarte, T. R. (2000). Cellular and subcellular localization of peripheral benzodiazepine receptors after trimethyltin neurotoxicity. *Journal of Neurochemistry*, *74*(4), 1694–1704. https://doi.org/10.1046/j.1471-4159.2000.0741694.x

Lavisse, S., Guillermier, M., Hérard, A. S., Petit, F., Delahaye, M., Van Camp, N. V., Haim, L. B., Lebon, V., Remy, P., Dollé, F., Delzescaux, T., Bonvento, G., Hantraye, P., & Escartin, C. (2012). Reactive astrocytes overexpress TSPO and are detected by TSPO positron emission tomography imaging. *The Journal of Neuroscience*, *32*(32), 10809–10818. https://doi.org/10.1523/JNEUROSCI.1487-12.2012

Lee, K., Kerner, J., & Hoppel, C. L. (2011). Mitochondrial carnitine palmitoyltransferase 1a (CPT1a) is part of an outer membrane fatty acid transfer complex. *Journal of Biological Chemistry*, *286*(29), 25655–25662. https://doi.org/10.1074/jbc.M111.228692

Lee, Y., Park, Y., Nam, H., Lee, J. W., & Yu, S. W. (2020). Translocator protein (TSPO): The new story of the old protein in neuroinflammation. *BMB Reports*, *53*(1), 20–27. https://doi.org/10.5483/BMBRep.2020.53.1.273

Li, M., Ren, H., Sheth, K. N., Shi, F. D., & Liu, Q. (2017). A TSPO ligand attenuates brain injury after intracerebral hemorrhage. *The FASEB Journal*, *31*(8), 3278–3287. https://doi.org/10.1096/fj.201601377RR

Li, Y., Chen, L., Li, L., Sottas, C., Petrillo, S. K., Lazaris, A., Metrakos, P., Wu, H., Ishida, Y., Saito, T., Golden-Mason, L., Rosen, H. R., Wolff, J. J., Silvescu, C. I., Garza, S., Cheung, G., Huang, T., Fan, J., Culty, M., … Papadopoulos, V. (2021). Cholesterol-binding translocator protein TSPO regulates steatosis and bile acid synthesis in nonalcoholic fatty liver disease. *iScience*, *24*(5), 102457. https://doi.org/10.1016/j.isci.2021.102457

Liang, K. (2023). Mitochondrial CPT1A: Insights into structure, function, and basis for drug development. *Frontiers in Pharmacology*, *14*(March), 1–14. https://doi.org/10.3389/fphar.2023.1160440

Liddelow, S. A., Guttenplan, K. A., Clarke, L. E., Bennett, F. C., Bohlen, C. J., Schirmer, L., Bennett, M. L., Münch, A. E., Chung, W. S., Peterson, T. C., Wilton, D. K., Frouin, A., Napier, B. A., Panicker, N., Kumar, M., Buckwalter, M. S., Rowitch, D. H., Dawson, V. L., Dawson, T. M., … Barres, B. A. (2017). Neurotoxic reactive astrocytes are induced by activated microglia. *Nature*, *541*(7638), 481–487. https://doi.org/10.1038/nature21029

Liddelow, S. A., Marsh, S. E., & Stevens, B. (2020). Microglia and astrocytes in disease: Dynamic duo or partners in crime? *Trends in Immunology*, *41*(9), 820–835. https://doi.org/10.1016/j.it.2020.07.006

Loth, M. K., Guariglia, S. R., Re, D. B., Perez, J., de Paiva, V. N., Dziedzic, J. L., Chambers, J. W., Azzam, D. J., & Guilarte, T. R. (2020). A novel interaction of translocator protein 18 kDa (TSPO) with NADPH oxidase in microglia. *Molecular Neurobiology*, *57*(11), 4467–4487. https://doi.org/10.1007/s12035-020-02042-w

Lu, M., Sun, X. L., Qiao, C., Liu, Y., Ding, J. H., & Hu, G. (2014). Uncoupling protein 2 deficiency aggravates astrocytic endoplasmic reticulum stress and nod-like receptor protein 3 inflammasome activation. *Neurobiology of Aging*, *35*(2), 421–430. https://doi.org/10.1016/j.neurobiolaging.2013.08.015

MacDonald, A. J., Holmes, F. E., Beall, C., Pickering, A. E., & Ellacott, K. L. J. (2020). Regulation of food intake by astrocytes in the brainstem dorsal vagal complex. *Glia*, *68*(6), 1241–1254. https://doi.org/10.1002/glia.23774

Mason, S. (2017). Lactate shuttles in neuroenergetics-homeostasis, allostasis and beyond. *Frontiers in Neuroscience*, *11*(February), 1–15. https://doi.org/10.3389/fnins.2017.00043

Moatti, A., & Cohen, J. L. (2021). The TNF-$\alpha$/TNFR2 pathway: Targeting a brake to release the anti-tumor immune response. *Frontiers in Cell and Development Biology*, *9*(October), 1–18. https://doi.org/10.3389/fcell.2021.725473

Monga, S., Denora, N., Laquintana, V., Franco, M., Marek, I., Singh, S., Nagler, R., Weizman, A., & Gavish, M. (2020). The protective effect of the TSPO ligands 2,4-Di-Cl-MGV-1, CB86, and CB204 against LPS-induced M1 pro-inflammatory activation of microglia. *Brain, Behavior, & Immunity—Health*, *5*(March), 1–10. https://doi.org/10.1016/j.bbih.2020.100083

Monga, S., Nagler, R., Amara, R., Weizman, A., & Gavish, M. (2019). Inhibitory effects of the two novel TSPO ligands 2-Cl-MGV-1 and MGV-1 on LPS-induced microglial activation. *Cell*, *8*, 8. https://doi.org/10.3390/cells8050486

Mookerjee, S. A., & Brand, M. D. (2015). Measurement and analysis of extracellular acid production to determine glycolytic rate. *Journal of Visualized Experiments*, *2015*(106), 1–9. https://doi.org/10.3791/53464

Mookerjee, S. A., Goncalves, R. L. S., Gerencser, A. A., Nicholls, D. G., & Brand, M. D. (2015). The contributions of respiration and glycolysis to extracellular acid production. *Biochimica et Biophysica Acta, Bioenergetics*, *1847*(2), 171–181. https://doi.org/10.1016/j.bbabio.2014.10.005

Morant-Ferrando, B., Jimenez-Blasco, D., Alonso-Batan, P., Agulla, J., Lapresa, R., Garcia-Rodriguez, D., Yunta-Sanchez, S., Lopez-Fabuel, I., Fernandez, E., Carmeliet, P., Almeida, A., Garcia-Macia, M., & Bolaños, J. P. (2023). Fatty acid oxidation organizes mitochondrial supercomplexes to sustain astrocytic ROS and cognition. *Nature Metabolism*, *5*(August), 1290–1302. https://doi.org/10.1038/s42255-023-00835-6

Morrissey, N. A., Beall, C., & Ellacott, K. L. J. (2021). Absence of the mitochondrial translocator protein 18 kDa in mice does not affect body weight or food intake responses to altered energy availability. *Journal of Neuroendocrinology*, *33*(9), 1–14. https://doi.org/10.1111/jne.13027

Muthuramu, I., Singh, N., Amin, R., & De Geest, B. (2015). Role of lipids and lipoproteins in myocardial biology and in the development of heart failure. *Clinical Lipidology*, *10*(4), 329–342. https://doi.org/10.2217/CLP.15.20

Notter, T., Schalbetter, S. M., Clifton, N. E., Mattei, D., Richetto, J., Thomas, K., Meyer, U., & Hall, J. (2021). Neuronal activity increases translocator protein (TSPO) levels. *Molecular Psychiatry*, *26*(6), 2025–2037. https://doi.org/10.1038/s41380-020-0745-1

Nutma, E., Ceyzériat, K., Amor, S., Tsartsalis, S., Millet, P., Owen, D. R., Papadopoulos, V., & Tournier, B. B. (2021). Cellular sources of TSPO expression in healthy and diseased brain. *European Journal of Nuclear Medicine and Molecular Imaging*, *49*(1), 146–163. https://doi.org/10.1007/s00259-020-05166-2

O'Neill, L. A. J., Kishton, R. J., & Rathmell, J. (2016). A guide to immunometabolism for immunologists. *Nature Reviews. Immunology*, *16*(9), 553–565. https://doi.org/10.1038/nri.2016.70

Ortinski, P. I., Reissner, K. J., Turner, J., Anderson, T. A., & Scimemi, A. (2022). Control of complex behavior by astrocytes and microglia. *Neuroscience & Biobehavioral Reviews*, *137*(January), 104651. https://doi.org/10.1016/j.neubiorev.2022.104651

Park, K., & Lee, S. J. (2020). Deciphering the star codings: Astrocyte manipulation alters mouse behavior. *Experimental & Molecular Medicine*, *52*(7), 1028–1038. https://doi.org/10.1038/s12276-020-0468-z

Raichle, M. E., & Gusnard, D. A. (2002). Appraising the brain's energy budget. *Proceedings of the National Academy of Sciences of the United States of America*, *99*(16), 10237–10239. https://doi.org/10.1073/pnas.172399499

Ran, F. A., Hsu, P. D., Wright, J., Agarwala, V., Scott, D. A., & Zhang, F. (2013). Genome engineering using the CRISPR-Cas9 system. *Nature Protocols*, *8*(11), 2281–2308. https://doi.org/10.1038/nprot.2013.143

Robb, J. L., Hammad, N. A., Weightman Potter, P. G., Chilton, J. K., Beall, C., & Ellacott, K. L. J. (2020). The metabolic response to inflammation in astrocytes is regulated by nuclear factor-kappa B signaling. *Glia*, *68*(11), 2246–2263. https://doi.org/10.1002/glia.23835

Robb, J. L., Morrissey, N. A., Weightman Potter, P. G., Smithers, H. E., Beall, C., & Ellacott, K. L. J. (2019). Immunometabolic changes in

glia—A potential role in the pathophysiology of obesity and diabetes. *Neuroscience*, *2020*(447), 167–181. https://doi.org/10.1016/j.neuroscience.2019.10.021

Schindelin, J., Arganda-Carreras, I., Frise, E., Kaynig, V., Longair, M., Pietzsch, T., Preibisch, S., Rueden, C., Saalfeld, S., Schmid, B., Tinevez, J. Y., White, D. J., Hartenstein, V., Eliceiri, K., Tomancak, P., & Cardona, A. (2012). Fiji: An open-source platform for biological-image analysis. *Nature Methods*, *9*(7), 676–682. https://doi.org/10.1038/nmeth.2019

Schlaepfer, I. R., & Joshi, M. (2020). CPT1A-mediated fat oxidation, mechanisms, and therapeutic potential. *Endocrinology*, *161*, bqz046. https://doi.org/10.1210/endocr/bqz046

Selvaraj, V., & Tu, L. N. (2016). Current status and future perspectives: TSPO in steroid neuroendocrinology. *The Journal of Endocrinology*, *231*(1), 1–30. https://doi.org/10.1530/JOE-16-0241

Shehadeh, M., Palzur, E., Apel, L., & Soustiel, J. F. (2019). Reduction of traumatic brain damage by Tspo ligand etifoxine. *International Journal of Molecular Sciences*, *20*(11), 2639. https://doi.org/10.3390/ijms20112639

Stanke, K. M., Wilson, C., & Kidambi, S. (2021). High expression of glycolytic genes in clinical glioblastoma patients correlates with lower survival. *Frontiers in Molecular Biosciences*, *8*(December), 1–12. https://doi.org/10.3389/fmolb.2021.752404

Takahashi, E., & Yamaoka, Y. (2017). Simple and inexpensive technique for measuring oxygen consumption rate in adherent cultured cells. *The Journal of Physiological Sciences*, *67*(6), 731–737. https://doi.org/10.1007/s12576-017-0563-7

Tournier, B. B., Bouteldja, F., Amoss, Q., Nicolaides, A., Azevedo, M. D., Tenenbaum, L., Garibotto, V., Ceyzériat, K., & Millet, P. (2023). 18 kDa translocator protein TSPO is a mediator of astrocyte reactivity. *ACS Omega*, *8*(34), 31225–31236. https://doi.org/10.1021/acsomega.3c03368

Tournier, B. B., Tsartsalis, S., & Ceyz, K. (2020). Astrocytic TSPO up-regulation appears before microglial TSPO in Alzheimer's disease. *Journal of Alzheimer's Disease*, *77*, 1043–1056. https://doi.org/10.3233/JAD-200136

Tu, L. N., Morohaku, K., Manna, P. R., Pelton, S. H., Butler, W. R., Stocco, D. M., & Selvaraj, V. (2014). Peripheral benzodiazepine receptor/translocator protein global knock-out mice are viable with no effects on steroid hormone biosynthesis. *The Journal of Biological Chemistry*, *289*(40), 27444–27454. https://doi.org/10.1074/jbc.M114.578286

Tu, L. N., Zhao, A. H., Hussein, M., Stocco, D. M., & Selvaraj, V. (2016). Translocator protein (TSPO) affects mitochondrial fatty acid oxidation in steroidogenic cells. *Endocrinology*, *157*(3), 1110–1121. https://doi.org/10.1210/en.2015-1795

U-373 MG (Uppsala) (ECACC 08061901) [Internet]. https://www.culturecollections.org.uk/products/celllines/generalcell/detail.jsp?refId=08061901&collection=ecacc_gc

Verkhratsky, A., & Nedergaard, M. (2018). Physiology of astroglia. *Physiological Reviews*, *98*(1), 239–389. https://doi.org/10.1152/physrev.00042.2016

Victorio, C. B. L., Msallam, R., Novera, W., Ong, J., Yang, T. J., Ganasarajah, A., Low, J., Watanabe, S., & Chacko, A. M. (2023). TSPO expression in a Zika virus murine infection model as an imaging target for acute infection-induced neuroinflammation. *European Journal of Nuclear Medicine and Molecular Imaging*, *50*(3), 742–755. https://doi.org/10.1007/s00259-022-06019-w

Weightman Potter, P. G., Vlachaki Walker, J. M., Robb, J. L., Chilton, J. K., Williamson, R., Randall, A. D., Ellacott, K. L. J., & Beall, C. (2019). Basal fatty acid oxidation increases after recurrent low glucose in human primary astrocytes. *Diabetologia*, *62*(1), 187–198. https://doi.org/10.1007/s00125-018-4744-6

Winkeler, A., Boisgard, R., Awde, A. R., Dubois, A., Thézé, B., Zheng, J., Ciobanu, L., Dollé, F., Viel, T., Jacobs, A. H., & Tavitian, B. (2012). The translocator protein ligand [18F]DPA-714 images glioma and activated microglia in vivo. *European Journal of Nuclear Medicine and Molecular Imaging*, *39*(5), 811–823. https://doi.org/10.1007/s00259-011-2041-4

Wolf, A., Herb, M., Schramm, M., & Langmann, T. (2020). The TSPO-NOX1 axis controls phagocyte-triggered pathological angiogenesis in the eye. *Nature Communications*, *11*(1), 1–17. https://doi.org/10.1038/s41467-020-16400-8

Wurm, J., Konttinen, H., Andressen, C., Malm, T., & Spittau, B. (2021). Microglia development and maturation and its implications for induction of microglia-like cells from human iPSCs. *International Journal of Molecular Sciences*, *22*(6), 1–13. https://doi.org/10.3390/ijms22063088

Xiong, X. Y., Tang, Y., & Yang, Q. W. (2022). Metabolic changes favor the activity and heterogeneity of reactive astrocytes. *Trends in Endocrinology and Metabolism*, *33*(6), 390–400. https://doi.org/10.1016/j.tem.2022.03.001

Yang, L., Qi, Y., & Yang, Y. (2015). Astrocytes control food intake by inhibiting AGRP neuron activity via adenosine A1 receptors. *Cell Reports*, *11*(5), 798–807. https://doi.org/10.1016/j.celrep.2015.04.002

Yao, R., Pan, R., Shang, C., Li, X., Cheng, J., Xu, J., & Li, Y. (2020). Translocator protein 18 kDa (TSPO) deficiency inhibits microglial activation and impairs mitochondrial function. *Frontiers in Pharmacology*, *11*, 1–10. https://doi.org/10.3389/fphar.2020.00986

Yin, F., Sancheti, H., Patil, I., & Cadenas, E. (2016). Energy metabolism and inflammation in brain aging and Alzheimer's disease. *Free Radical Biology & Medicine*, *100*, 108–122. https://doi.org/10.1016/j.freeradbiomed.2016.04.200

Zhang, H., Wang, H., Gao, F., Yang, J., Xu, Y., Fu, Y., Cai, M., Zhang, X., Yang, Q., Tong, K., Hu, Y., Chen, H., Ma, C., He, W., & Zhang, J. (2021). TSPO deficiency accelerates amyloid pathology and neuroinflammation by impairing microglial phagocytosis. *Neurobiology of Aging*, *106*, 292–303. https://doi.org/10.1016/j.neurobiolaging.2021.06.020

Zheng, D., Liwinski, T., & Elinav, E. (2020). Inflammasome activation and regulation: Toward a better understanding of complex mechanisms. *Cell Discovery*, *6*(1), 36. https://doi.org/10.1038/s41421-020-0167-x

Zhou, J., Zhang, X., Peng, J., Xie, Y., du, F., Guo, K., Feng, Y., Zhang, L., Chen, L., & Jiang, Y. (2020). TSPO ligand Ro5-4864 modulates microglia/macrophages polarization after subarachnoid hemorrhage in mice. *Neuroscience Letters*, *729*(April), 134977. https://doi.org/10.1016/j.neulet.2020.134977

Zhou, Z., Okamoto, K., Onodera, J., Hiragi, T., Andoh, M., Ikawa, M., Tanaka, K. F., Ikegaya, Y., & Koyama, R. (2021). Astrocytic cAMP modulates memory via synaptic plasticity. *Proceedings of the National Academy of Sciences of the United States of America*, *118*(3), 1–10. https://doi.org/10.1073/pnas.2016584118

## SUPPORTING INFORMATION

Additional supporting information can be found online in the Supporting Information section at the end of this article.

**How to cite this article:** Firth, W., Robb, J. L., Stewart, D., Pye, K. R., Bamford, R., Oguro-Ando, A., Beall, C., & Ellacott, K. L. J. (2024). Regulation of astrocyte metabolism by mitochondrial translocator protein 18 kDa. *Journal of Neurochemistry*, *00*, 1–28. https://doi.org/10.1111/jnc.16089